Received 27 June 2022; revised 23 July 2022; accepted 28 July 2022. Date of publication 2 August 2022; date of current version 12 August 2022.

Digital Object Identifier 10.1109/OJAP.2022.3195665

Wideband Reflectarrays for 5G/6G: A Survey

PANAGIOTIS IOANNIS THEOHARIS [1] (Graduate Student Member, IEEE), RAAD RAAD [1] (Member, IEEE), FAISEL TUBBAL [1,2] (Senior Member, IEEE), MUHAMMAD USMAN ALI KHAN [1,3] (Member, IEEE), AND ABBAS JAMALIPOUR [4] (Fellow, IEEE)

[1]School of Electrical, Computer and Telecommunications Engineering, University of Wollongong, Wollongong, NSW 2522, Australia

[2]Technological Project Department, Libyan Center for Remote Sensing and Space Technology, Tripoli, Libya

[3]Department of Electronics Engineering, The Islamia University of Bahawalpur, Bahawalpur 63100, Pakistan

[4]School of Electrical and Information Engineering, The University of Sydney, Sydney, NSW 2006, Australia

CORRESPONDING AUTHOR: P. I. THEOHARIS (e-mail: pit289@uowmail.edu.au)

IEEE OJAP encourages responsible authorship practices and the provision of information about the specific contribution of each author.

This work was supported by the Australian Government Research Training Program (AGRTP).

ABSTRACT Application demand for faster data rates is driving the need for wider operating bandwidth of future 5G/6G communication systems which in turn poses stringent requirements on the design of suitable antennas. A candidate antenna that can support 5G/6G systems are reflectarrays (RAs) due to their numerous potentials, such as high gain, beam shaping, beam scanning, reconfigurability and multi-beam characteristics. However, reflectarrays are usually limited by their narrowband characteristics. Hence, this work examines the state of the art of wideband reflectarrays. Wideband reflectarrays are reviewed and categorized according to four wideband phase tuning mechanisms. The bandwidth is reviewed and compared both from a unit cell and reflectarray system perspective with emphasis on the gain-bandwidth performance. Different wideband unit cell geometries are covered and grouped by the wideband phase tuning approach. The effect of each wideband phase tuning approach on the gain-bandwidth RA performance is then analyzed by considering the operating frequency, the reflection phase range, the substrate structure and material, the aperture size, the aperture efficiency, the focal distance, the cross-polarization performance as well as the gain and side lobe levels. Finally, the phase tuning approaches are compared against each other, and guidelines are provided for designing reflectarrays with wide gain-bandwidth.

INDEX TERMS 5G, 6G, reflectarrays, wideband, gain-bandwidth.

I. INTRODUCTION

THE EVOLUTION of wireless communication from the first generation (1G) systems until the fourth generation (4G) is characterized by improvements due to demands in the capacity, the throughput, the reliability and the latency of wireless systems [1]. These demands dictate the key enabling technologies of each generation of wireless communication system with the latest generations being 5G and the upcoming 6G. More specifically, the demands set by the 5G systems are 1-10 Gbps of throughput, reduced end-to-end latency of 1ms, 10-100 times increase in the number of connected devices, high availability, thousand-fold improvement in capacity and 100% coverage [2], [3]. Pushing the limits even further, future 6G systems must support peak data rates in excess of 1Tbps which is a tenfold increase of the 5G counterpart [4]. The minimum communication plane latency must be 25ns while user mobilities of up to 1000km/h must be considered as in the case of airborne terminals. Accordingly, the Internet of things (IoT) which is envisioned as a 5G application will be considered to be Internet of Everything with a tenfold increase in the connection density of 6G. To meet these demands, 5G/6G technologies require migration to higher frequency bands such as mm-Wave for 5G and up to 1 THz for 6G. In addition, 6G applications might be benefited by migrating from a fixed to a dynamic spectrum allocation [5].

A. ANTENNAS FOR 5G/6G APPLICATIONS

From an electromagnetic point of view, a 5G/6G communication system that satisfies the aforementioned requirements, poses many challenges during the design and integration of antennas either in mobile or fixed terminals. The operating bandwidth of 5G/6G is mainly dependent on the frequency band of interest, namely sub-6GHz (FR1), mm-Wave (FR2) or THz. For instance, at FR1 an operating bandwidth of approximately 400MHz is required while at FR2 or THz the operating bandwidths can reach up to 3.25GHz or 10-100GHz, respectively [4]. Furthermore, at mm-Wave/THz frequencies the electromagnetic wave may undergo a significant degradation such as blockage or bouncing and path loss attenuation impairing the Signal-to Interference-plus Noise ratio of the link (SINR) unless a high gain antenna system is used [6]. On the other hand, when using highly directional antennas, the benefit of wide user coverage is violated unless multibeam antennas are considered. Consequently, highly directional antennas equipped with adaptive beamforming as well as Multiple Input Multiple Output (MIMO) capabilities must be used [1], [7]. In addition, mobile terminals such as trains or airplanes that have high velocity poses a real challenge in terms of base stations or user demand tracking in order to meet and adapt to diverse 5G/6G traffic [8]. Therefore, beam steering and beamforming antenna architectures are inseparable design requirement of 5G/6G communication systems [5]. Furthermore, adaptive beamforming and steerability are required to accommodate rapidly time-varying traffic as well as the on-demand beam coverage due to the spatial evolution of the users [9]. As a result, 5G/6G antennas should have a reconfigurable radiation pattern and superior gain bandwidth performance [10]. Apart from that, null-steering control can also be employed to suppress the interference caused by resource sharing maintaining a good impedance matching and gain bandwidth during the scanning of the beam. Finally, a polarization diverse antenna system with high polarization purity and wide axial ratio bandwidth can be implemented to vastly increase the throughput of the overall system by sending signals at the same frequency with different polarizations.

Traditionally microstrip antennas have been employed in 4G systems [11]. While the aforementioned 5G/6G antenna characteristics require a versatile and reconfigurable antenna type such as active phased arrays [7]. However, phased arrays have one of the most power demanding antenna architectures due to their complex feeding systems [12]. Moreover, quasi optical beamforming technologies such as lens antennas are promising solutions for 6G applications where the operating frequency lies in the low THz range. Nevertheless, this type of antennas is normally bulky and heavy [13]. A viable alternative for 5G/6G systems could be reflectarrays [13]. Reflectarray is an emerging antenna architecture considered as a hybrid of reflector and phased antenna arrays [14], [15]. Reflectarrays (RAs) combine the advantages and at the same time they don't inherit any of the drawbacks of both reflector antennas and phased arrays. RAs provide high gain, beam shaping ability, radiation pattern reconfigurability, scanning and multi-beam potentials [16], [17]. Compared to phased arrays, RAs don't require a complex and lossy feeding network which may result in higher aperture efficiencies due to reduced losses [13]. The other advantage of planar RAs is that they are lightweight and exhibit a low profile [12]. Reflectarrays have been used traditionally on large satellite platforms to realize either pencil or shaped beams in a variety of space missions [18]–[22]. RAs have also been considered as smart solutions for future Non-Terrestrial-Networks (NTN) supported by Low Earth Orbit (LEO) mega constellations to provide shaped-beam isoflux patterns for the user at Ku-band with 2 GHz bandwidth [23]. When it comes to small satellite applications, RAs have been employed in the Integrated Solar Array and Reflectarray (ISARA) where high-gain Ka-band CubeSat communications were demonstrated and the deep space CubeSat MarCO mission implemented by NASA Jet Propulsion Laboratory [24], [25]. Moreover, RAs have been proposed as CubeSat antenna candidates for circular polarized intersatellite links where the weight and profile of the antenna are of great significance [26]. More recently, reflectarrays have been considered for 5G/6G communications to provide both electronic and mechanical beam steering at FR1 and FR2 frequency ranges, respectively [27], [28] as well as dual band and dual polarization capabilities [29]. In addition, beamsteering at the THz ranges has been demonstrated by [30] only be using resonant phase gradient elements. Furthermore, reflectarrays have also been studied as strong candidates for Reconfigurable Intelligent Surfaces (RIS) where the 5G/6G communication channel can be manipulated [31]. The application of RAs for 6G RIS has been investigated by where a liquid crystal 108GHz RA that has demonstrated 6G beamforming, steering and splitting [32]. Another 5G/6G application that RAs is the Internet of Vehicles, where a single RA aperture operating from 10-30GHz was able to cover six different frequency bands [33]. The feasibility of RAs as 5G Ka-band fronthaul base stations for indoor and outdoor environments have been studied where the antenna demonstrated both near and far field capabilities, respectively [13]. Finally, a 400GHz polarization diverse quartz-based RA has been proposed by [34] for high speed 6G links inside a high density base station. These works showcase the enormous capabilities of reflectarrays as strong candidates for 5G and future 6G applications. Nevertheless, reflectarrays have some limitations such as narrow bandwidth, e.g., less than 10%, the requirement of active elements to achieve beam scanning ability and their high fabricating cost due to the use of low loss tangent dielectric substrates [12], [35].

B. RELATED WORKS AND CONTRIBUTION OF THIS PAPER

As shown in Table 1, RAs have been reviewed from different perspectives. In 2014, Hum and Perruisseau-Carrier [12],

TABLE 1. Existing review articles on reflectarrays.

Reference	Year	RAs studied or categorized based on
Hum *et al.*[12]	2014	*Different mechanisms of reconfigurability.*
Nayeri *et al.*[36]	2015	*Beam-Scanning architectures, techniques and enabling technologies.*
Dahri *et al.*[16]	2017	*Bandwidth enhancement techniques for 5G.*
Dahri *et al.*[17]	2018	*Element types and RA system level design for high gain and efficiency for 5G.*
Dahri *et al.*[37]	2018	*Polarization type for polarization diversity and enabling technologies for adaptive beam steering for 5G.*
Dahri *et al.*[38]	2020	*The element type, the feeding structure, and the aperture shape for efficiency characterization and measurement.*
This paper	2022	*Techniques, element types and full RA architectures for wideband RAs considering the RA level performance as candidates for 5G/6G*

reviews various techniques and approaches for designing reconfigurable RAs with a focus on beam forming and beam steering. Moreover, reconfigurability was also examined based on polarization flexible and frequency agile unit cells. In addition, active RAs with integrated amplifiers that can achieve a reflection coefficient magnitude greater that unity were also studied. In 2015, Nayeri *et al.* [36], several beam-scanning methodologies and enabling technologies were also surveyed and categorized into two major sets, namely, the feed tuning and the aperture phase-tuning techniques. The authors also focused on active RAs and investigated different ways to achieve phase control such as analog, digital or subarray techniques. Then in 2017 and 2018 a number of reviews articles appeared that looked at RAs from a 5G perspective. This is contained in the works of Dahri et.al. from 2017 to 2020 [16], [17], [37] and [38]. In these works, the authors reviewed different bandwidth enhancement techniques for wideband 5G RAs by considering different element geometries under each technique [16]. In addition, high gain and high efficiency RAs have been investigated from an element point of view as well as full RA systems. This includes feeding mechanisms, RA combined with sub reflectors and also the material used for manufacturing the RA [17]. The survey [17] was further extended in [38] by the same authors considering different element geometries, feeding structures and aperture shapes to quantify the loss and enhancement of the efficiency and the measurement accuracy of RAs. Finally, the work in [37] explored polarization diversity of RAs by categorizing the techniques based on the polarization type namely, dual linear and dual circular. Furthermore, the authors also investigated the RAs with adaptive beam-steering capabilities subdividing the study into two groups namely, electronically tunable materials and lumped components.

In this paper, we review wideband RAs that are suitable for 5G/6G applications. To the best of our knowledge, no previous work has made this contribution. The use of existing RAs as the enabling technology of 5G/6G systems has not been surveyed or reviewed so far in the existing literature.

To this end, this survey is aimed at investigating the gain-bandwidth performance of RAs from 5G/6G perspective. This is of great importance when considering RAs as candidates for future 5G/6G systems since high gain performance must be maintained over a wide operating frequency band within acceptable limits. More specifically, wideband RA architectures are surveyed in this paper. Initially, the wideband performance is categorized based on 4 main axes namely, tunable resonator including single and multilayer structures, element angular rotation, true time or phase delay lines and subwavelength periodicity. The 4 design techniques are investigated from a unit cell standpoint and then the full reflectarray system performance is considered and evaluated. More specifically, in the full system performance, the following metrics are considered, peak side lobe levels (SLL), cross polarization levels (X-Pol), aperture efficiency (AE), 1-dB gain bandwidth (BW), gain, aperture size, substrate material, number of layers, polarization type, phase reflection range and operating frequency band. The remainder of this paper has the following structure. Section II gives a background on reflectarrays including their operating principle and the evolution of wideband reflectarrays by capturing the timeline of the appearance of different wideband techniques. Section III presents an analysis on wideband phase tuning approaches of the unit cells. Section IV provides a discussion considering the full reflectarray performance. The paper concludes with Section V. The overall structure of this paper is shown in Fig. 1.

II. REFLECTARRAYS BACKGROUND

A. OPERATING PRINCIPLE

The basic building blocks of a printed microstrip reflectarray (RA) are a feeding system and a reflective planar surface placed on a grounded dielectric slab comprised by non-identical unit cells [39] see Fig. 2. The planar surface of the RA lies on the far field of the feeder so that the reflective surface is illuminated by a uniform plane wave for different angles of incidence given by equation (1).

$$\vec{E}_i(\vec{r}) = \vec{P}_i e^{-j\vec{k}\cdot\vec{R_i}} \tag{1}$$

Here, the harmonic oscillation term $e^{-j\omega t}$ is omitted from the expressions, $\vec{P}_i$ is the polarisation vector and conveys information about the magnitude and polarization of the incident electric field $\vec{E}_i$, the wave vector is represented by $\vec{k}$ and $\vec{R_i}$ is the position vector of the i^{th} element defined from the feeding antenna phase center.

The RA elements as seen in Fig. 2, may vary in shape and size and their purpose is to collimate the radiation from

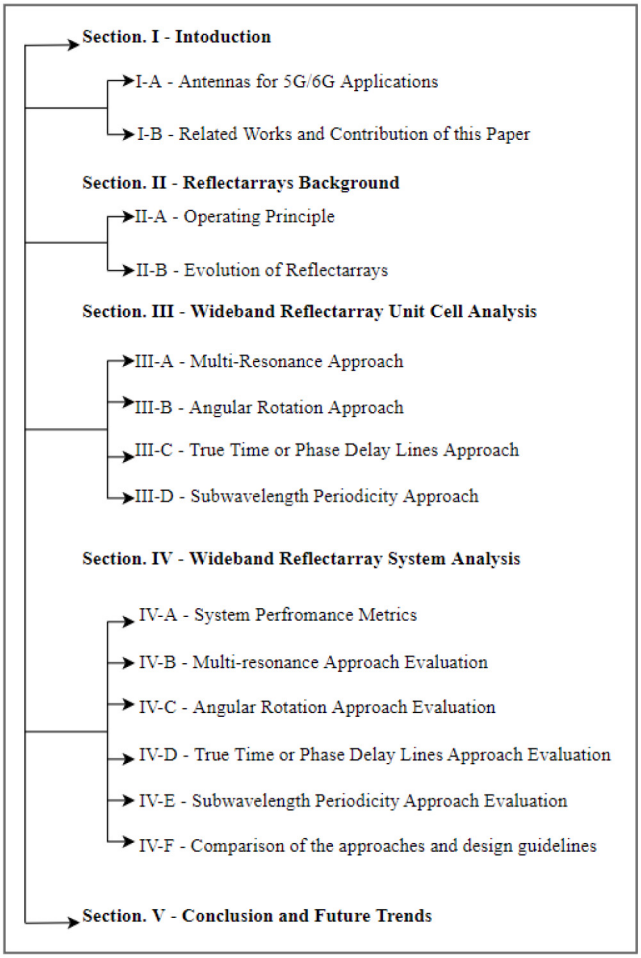

FIGURE 1. Structure of this survey.

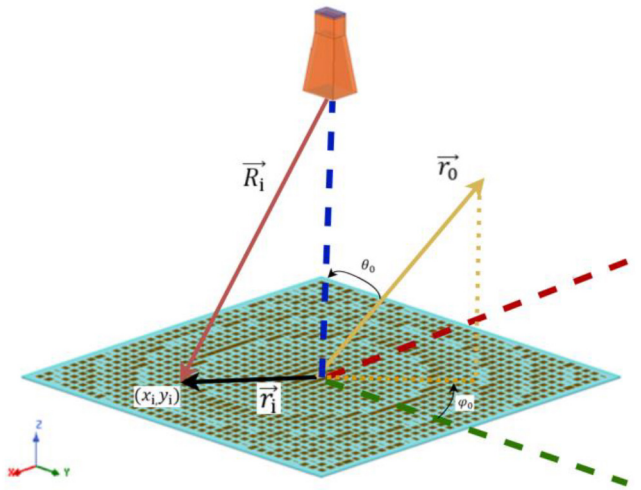

FIGURE 2. Geometry of a planar reflectarray antenna.

the feeding antenna in a desired direction $\vec{r_o}$ with a desired shape. To achieve that, the elements must introduce a phase shift $\Delta\phi_i$ between the incident $\vec{E}_i$ and reflected $\vec{E}_r$ fields. This process resembles the principal of a parabolic reflector antenna where the beam collimation is achieved by introducing a spatial phase delay due to the parabolic shape of the aperture.

Similar to planar arrays, if a broadside beam is required, a uniform phase distribution must be applied to the aperture. On the other hand, if the beam must be scanned in any a direction $\vec{r_o}$ then a progressive phase profile is required across the aperture. The incident electromagnetic wave on the aperture presents a phase profile proportional to the distance between the phase center of the feed antenna and the reflectarray element. This is called spatial phase delay and is given by equation (2):

$$\varphi_{sd} = -k_0 R_i \tag{2}$$

where R_i is the distance between the phase center of the feed antenna and the i^{th} scatterer and k_0 represents the free space wavenumber. To point the beam in a specific direction, a progressive phase profile φ_{pp} must be applied to the aperture given by equation (3),

$$\varphi_{pp} = -k_0 \vec{r_i} \cdot \hat{r}_0 = -k_0 (x_i \sin\theta_0 \cos\varphi_0 + y_i \sin\theta_0 \sin\varphi_0) \tag{3}$$

where (θ_0, φ_0) is the direction of the beam in spherical coordinates, (x_i, y_i) is the cartesian position in the x-y plane of the i^{th} element inside the aperture and $\hat{r}_0$ denotes the unit vector in the direction of the main beam. The final phase shift $\Delta\phi_i$ to get a pencil beam pointing at (θ_0, φ_0) can be found by compensating for the spatial phase delay introduced by the feeding antenna as shown in equation (4),

$$\Delta\phi_i = \varphi_{sd} - \varphi_{pp} + \varphi_c \tag{4}$$

where $\varphi_c = 2\pi N$ for $N = 0, 1, 2, \ldots$ is a phase constant accounting for the relative phase between the elements

B. EVOLUTION OF REFLECTARRAYS

In Fig. 3 the evolution of RAs since 1963 is presented. As it can be seen, first RA antenna was introduced in 1963 by Berry *et al.* [40] and consisted of an array of rectangular shorted waveguides with variable lengths. It was shown that the reflecting surface of an RA could be used to synthesize a surface impedance to produce the desired radiation pattern. It wasn't until the breakthrough of the printed circuit technology around 1977 when Malagisi [41] used electronically controlled microstrip circular patches antenna to construct the first printed RA surface. Following that, in 1992, Metzler [42] investigated for the first time the use of stub loaded microstrip reflectarray elements. A relationship between the length of the stubs with the phase and amplitude of the scattered field was established and verified experimentally using a C-band microstrip RA. In 1993, Pozar and Metzler [43], introduced a new approach of tuning the phase of the RA elements by varying their resonant length. Later, in 1998 Huang and Pogorzelski [39], demonstrated for the first time the use of elements with variable rotation angles for circular polarized RAs. This concept was

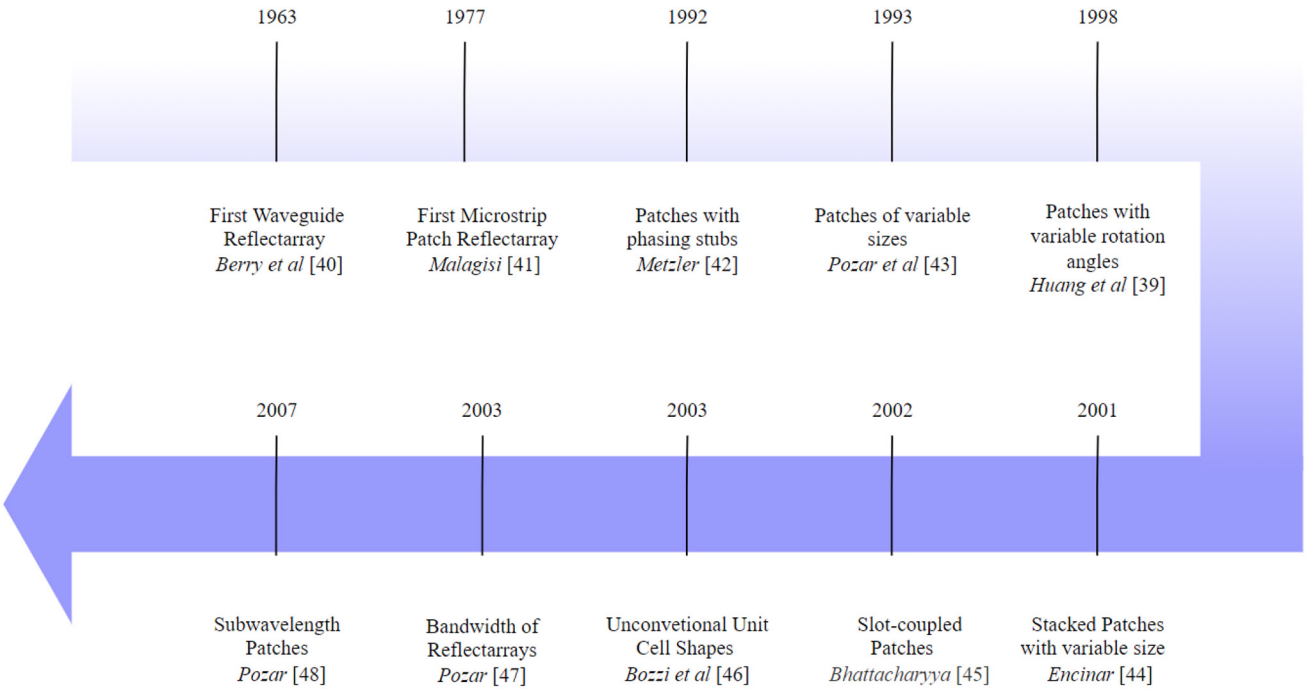

FIGURE 3. Timeline of when the different wideband approaches appeared.

demonstrated by fabricating two of the largest RAs at that time, operating at Ka-band. However, the achieved 1-dB gain bandwidth was only 3% at 32GHz. One of the first attempts to enhance the gain bandwidth performance of RAs was recorded in 2001 by Encinar [44]. The author used dual layer patches of variable size providing a 1-dB gain bandwidth of 16.7%. Moreover, in 2002, Bhattacharyya [45] used a slot-coupled square patch to a strip line. The 1-dB gain bandwidth was improved from 8.2% for the conventional patch to 12.5% for the slot-coupled patch element at 2GHz. The first attempt to evaluate the use of unconventional shapes as RA elements was in 2003 by Bozzi *et al.* [46]. Figure of merits to evaluate the RA elements such as the reflection phase sensitivity, the element bandwidth and cross polarization levels were defined for the first time. The authors investigated and compared the reflection properties of novel RA element shapes such as rectangles, dipoles and slotted patches versus their geometrical characteristics. Along similar lines, in 2003, Pozar [47], studied the RA system bandwidth. It was concluded that the element bandwidth greatly affects the full RA bandwidth for small and medium sized apertures, while the non-constant path delays become more dominant in large RAs. The concept of subwavelength RA elements was introduced in 2007 by Pozar [48] and was proven that using single layer subwavelength printed elements, the 1-dB gain bandwidth can exceed 20%.

This historical overview of the evolution of RA captures important points in the timeline that all the different fundamental wideband phase tuning mechanisms appeared for the first time. Since 2007, numerous variations of the fundamental approaches have already been proposed and they will be further investigated in Section III.

III. WIDEBAND REFLECTARRAY UNIT CELL ANALYSIS

A wideband antenna operation is crucial for 5G/6G systems [4], [16], [29]. However, one of the main limitations of the reflectarrays is their narrowband characteristic where a typical bandwidth does not exceed 10% [49]. Designing wideband microstrip reflectarrays is a challenging task due to two major factors, namely the element geometry [12], [16], [50] and the nature of the flat reflective surface that may cause non-constant phase delay paths across very large reflectarrays [47]. The RA bandwidth depends highly on the element's resonance which can provide the range of the phase shift. Consequently, the phase tuning range as well as any phase errors introduced as a function of frequency might degrade the bandwidth of the reflectarray. There are four main design approaches that exist so far and can be followed to implement wideband RA unit cells. These approaches are summarized in the diagram presented in Fig. 4 and are as follows:

1) Multi-Resonance
2) Angular Rotation
3) True Time or Phase Delay Lines
4) Subwavelength Periodicity

The remainder of Section III reviews different contributions from the literature for different RA unit cell geometries for wideband performance categorized based on the 4 aforementioned approaches. Emphasis is given on how the reflection phase response is dictated by variations in the unit cell structure and geometry.

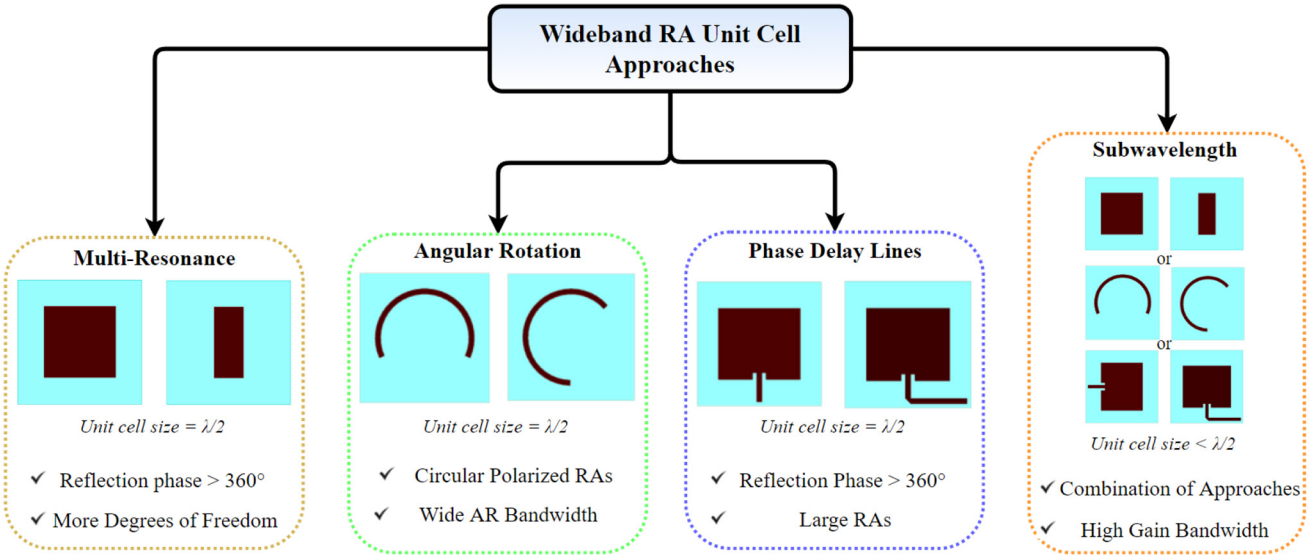

FIGURE 4. Design approaches for wideband RA unit cells.

A. MULTI-RESONANCE APPROACH

In the multi-resonance approach, the physical dimensions of the unit cell vary, hence the resonance frequency of the elements is changing, affecting both the reflected phase and magnitude. As a result, elements with different sizes will scatter or reradiate the incident field with different phases at a specific operating frequency. However, due to the high Q nature of printed antennas, the reflection phase response versus the element dimensions (also known as S-curve), presents a non-linearity around its resonant region. The non-linearity of the S-curve leads to strict manufacturing tolerances as the phase distribution across the RA is frequency dependent. Hence, the smoothness of the S-curve as well as the frequency dependence of reflected phase is an indication of how wide the element's bandwidth is.

Generally, a set of parallel linear reflection phase responses each corresponding to a different frequency shows the bandwidth performance of the RA element [49], [51] as seen in Fig. 5. It is important to mention that the phase range also depends on the substrate's thickness where an electrically thick substrate provides a wideband operation but at the same time will limit phase swing [52], [53]. For instance, a substrate thickness of $\lambda/10$ gives a phase reflection range of approximately 300° [44]. To achieve a linear S-curve and adequate reflection phase range of 360°, multiple resonances must be combined together either in multi- or single layer configuration. The concept of multilayer unit cell where each layer can produce several resonances is shown in Fig. 6. This leads to the generation of additional phase cycles and as a result a phase swing exceeding 360° can be obtained. This allows for thick substrates which consequently will smoothen the behavior of the reflected phase versus variations in geometry of the element.

For example, in the order of 2000, rectangular patches of variable sizes have been used as building blocks of multilayer

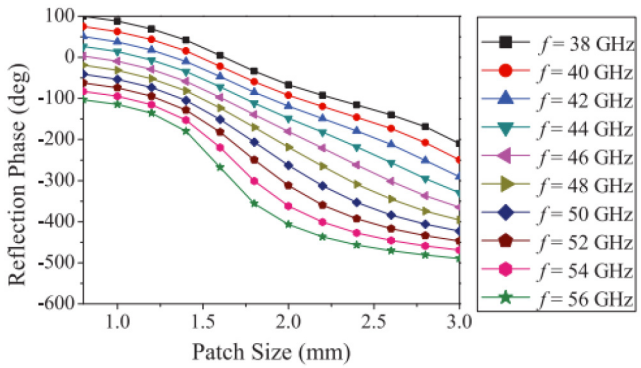

FIGURE 5. Reflection phase response versus patch size for different frequencies [54].

wideband RAs by Encinar *et al.* [44], [55]. The patches were arranged either in a 2-layer or 3-layer configuration, see Fig. 6 (b) and (c). Comparing these two architectures, a 400° increase can be achieved in the reflection phase range when the number of layers is increased from 2 to 3-layers. This is shown in [55] where a 3-layer RA achieved a reflection phase range of 800° by generating three resonant frequencies. The multilayer design used honeycomb lattice as substrates obtaining a bandwidth of 10% which is good for a 1-m RA. The 3-layer unit cell in [55] was successfully used to design a RA for Direct Broadcast Satellite Applications in 2011 by Encinar *et al.* [56]. Another multilayer RA based on T-shaped elements is presented in [57] by Ren *et al.* is shown in Fig. 6 (a). The dual layer RA provides a phase swing in the excess of 400° and a bandwidth improvement of 4% against the traditional dual layer square patch. Additionally, the T-shaped patch has the ability to transform LP incident waves into CP waves, thanks to the properly sized T branches.

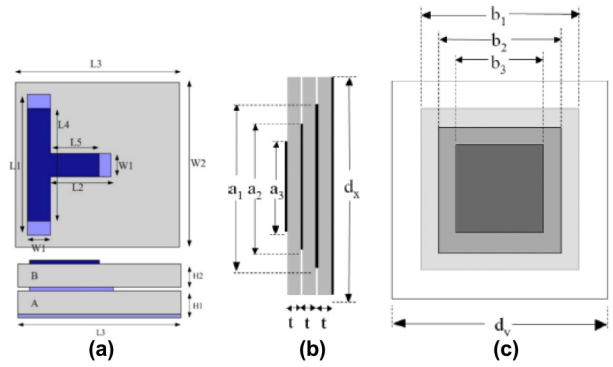

FIGURE 6. Multilayer Unit Cell Concept based on (a) T-shaped element [57] and rectangular patches (b) side view (c) top view [56].

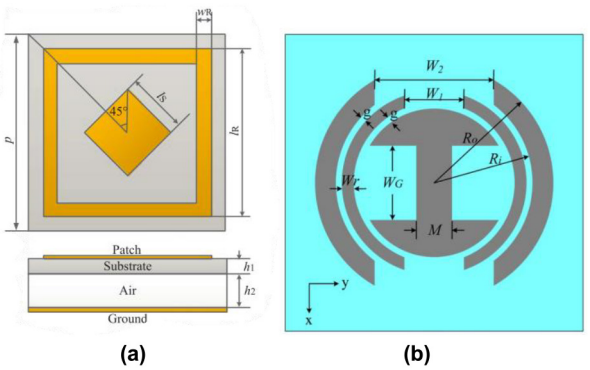

FIGURE 8. Multi-resonant element of (a) Dual Resonance Square Patch [54] and (b) Double Split Ring with I-shaped dipole [63].

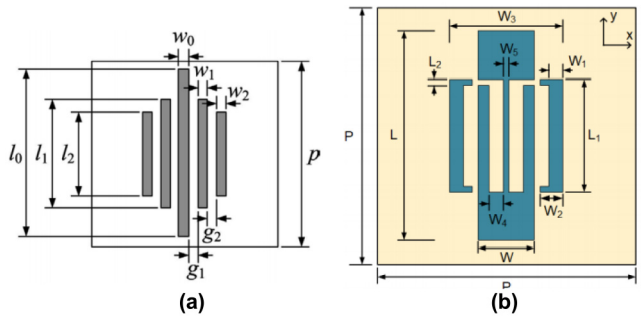

FIGURE 7. Multi-resonant element of (a) parallel dipoles [60] and (b) slotted patch with concave arms [61].

Instead of stacking different RAs, a more cost effective and simple design approach that can provide a wide bandwidth is using a single layer structure where each element can generate multiple resonances [16]. In 2007, a square slotted patch was proposed by Vita *et al.* [58] also known as the modified Malta cross increased the bandwidth to 19% using a single layer structure in a medium sized RA. Moreover, another multi-resonant structure can be considered an array of printed parallel dipoles with variable lengths where each dipole will resonate at a different frequency, thus producing a larger phase swing as shown in Fig. 7 (a). This technique was used by Li et. al and Yoon et. al in 2009 and 2015, respectively [59], [60]. Increasing the number of dipoles will produce a larger phase swing, e.g., from 3 to 5 dipoles per element, the phase range can be increased from 528° up to 800° and the bandwidth from 14.1% to 33.41%.

In 2010, Chaharmir *et al.* [62], introduced the use of cross-shaped concentric loops, as well as open rectangular concentric loops to design a dual-band broadband RA. The rectangular shaped elements are used for transmission while the crossed shaped ones for reception. The RA achieves a bandwidth of 12% and phase swing greater than 500° which can be tuned by adjusting the gap between the loops. Recently in 2019, Min and Guo [61], proposed a similar design including a slotted patch with concave arms that can also be used as a wideband unit cell as shown in Fig. 7 (b). Adding and adjusting the lengths of the concave arms, the extra required resonance is generated that can boost the phase swing to 400° and the bandwidth to 32%. In 2017 Xia *et al.* [54] tried to increase the linearity of the S-curve instead of achieving a phase range in the excess of 360°. A square loop and a rotated square patch as illustrated in Fig. 8 (a) was used to obtain dual resonance and hence an approximately straight reflection phase response from 0 to 360°. A combination of air and dielectric was used as substrate with an achievable bandwidth of 29.3%.

Multi-resonance can also be obtained by using a combination of ring-shaped, I-shaped printed dipoles and split ring elements which can still maintain linear polarization across the reflectarray as introduced by Chen *et al.* around 2012 [63], [64]. Tuning the widths of the parasitic printed split rings and dipoles as well as the radius of the ring, phase ranges of 400° can be achieved with a bandwidth in the excess of 22%, see Fig. 8 (b). More recent single-layer RA element designs that enhance the bandwidth use more sophisticated shapes such as the four-arm Archimedean spiral from Xue *et al.* in 2017 [65] where the length of each arm is tuned to provide a wide linear reflection phase range of 540° from 11.58GHz to 15.58GHz.

Moreover, in 2019 Karimipour and Aryanian introduced a novel synthesis method for wideband RA unit cell based on the system-by-design (SbD) paradigm [21]. The unit cell boundaries are defined based on the continuous genetic algorithm (CGA) which are then smoothed according to the spline technique. By utilizing this method, a unit cell with a reflection phase range of 450° was synthesized. The authors claim that the proposed synthesis method could reduce the manufacturing inaccuracies since the unit cell has minimum discontinuities. Also, this method can be applied for designing multiband unit-cell independent from their polarization state.

The concept of wideband RA unit cells with many degrees of freedom was introduced by Li *et al.* [66] in 2021. The authors proposed a spiral dipole loaded with 4 symmetrical

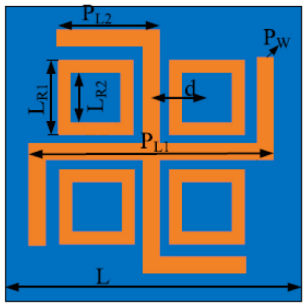

FIGURE 9. Spiral dipoles with rectangular ring TDF unit cell [66].

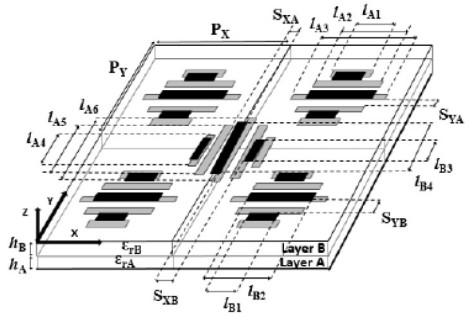

FIGURE 10. Printed parallel stacked dipoles in a periodic arrangement [69].

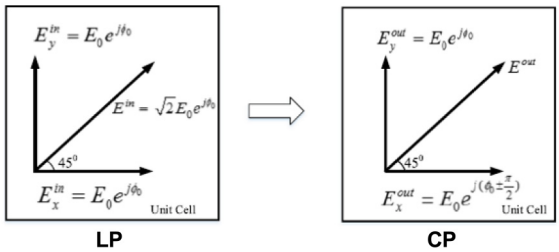

FIGURE 11. Linear to Circular Polarization conversion concept [73].

square ring as depicted in Fig. 9. The first degree of freedom (FDF) corresponds to the length of the main cross dipole and the second degree of freedom (SDF) to the length of the spiral arm. By utilizing the FDF, only 320° reflected phase range can be achieved while by continuously adjusting the SDF an additional 40° is obtained. Furthermore, the 4 rectangular rings can effectively reduce the slope of the reflected phase and achieve an almost linear response. Consequently, the TDF unit cell achieved a full 360° phase shift and was used as a building block for an X-band RA maintain a 1dB gain drop from 6.6-9.4 GHz. As a final remark, wideband unit cells can be realized by utilizing the degrees of freedom offered by the corresponding geometry to introduce additional resonances. This can yield a linear reflection phase variation exceeding 360° which is an essential requirement for wideband RAs.

Furthermore, achieving wideband performance in dual polarization would be an indispensable feature for both mm-Wave and sub-6GHz 5G/6G base stations [67], [68]. This would allow for communication at the same frequency band but in orthogonal polarizations, vastly increasing the throughput of the system. Polarization diversity, flexibility or multiple-polarization capability can be defined in the sense that a RA can produce two different polarizations at a single or multiple frequency bands. For example, in the case of Linear Polarization (LP), dual LP can be achieved in a single frequency band, e.g. Ku-band resulting in two beams, namely an X- and Y- polarized one [69]. Accordingly, a RA can achieve dual LP in two different frequency bands such as X-pol in K-band and Y-polarization in X-band [70].

A popular unit-cell for independent control of each orthogonal polarization in the same or even separate frequency bands is the set of printed parallel stacked dipoles [19], [69], [71]. In [19] different arrangements of printed dipoles were studied for independent phase control in each polarization. It was stressed out that there must be symmetry within the unit-cell so that the cross-polarization levels are kept low. Furthermore, as the number of dipoles is increased, the degrees of freedom in terms of resonances can be increased, thus improving the element bandwidth. The resonances, and hence the reflection phase range of each polarization is directly related to the lengths of the parallel dipoles. Best performance was obtained with 3 degrees of freedom per polarization in a two-layer RA allowing for different beams per polarization. The proposed unit cell achieved a linear reflection phase response exceeding 720° by varying the length of the central dipole. Moreover, a similar implementation can be found in [69] where each orthogonal polarization can be controlled independently in Ku- and Ka-band. The unit cell consists of 2 sets of stacked dipoles as shown in Fig. 10, placed at 0.6λ grid spacing at the higher frequency to avoid grating lobes. Changing the length of dipoles along the x-axis will control the H polarized wave while changing the lengths along the y-axis will control the V polarized wave. In the 2-layer configuration, the lower layer controls the Ku-band polarizations while upper layer is responsible for the Ka-band. The proposed unit cell achieved a 400° and 500° reflected phase swing at 12 and 19.5GHz, respectively.

B. ANGULAR ROTATION APPROACH

In several satellite applications, the design of circularly or reflectarray antennas is mandatory to enable high-data rate and broadband communication. In addition, employing a circularly polarized reflectarray antenna on board the satellite can make the communication immune to multipath effects, polarization mismatching due to antenna misalignment and the "Faraday rotation" that can alter the polarization of waves passing the atmosphere [72]. There are two existing approaches to achieve a CP collimated beam from a reflectarray, namely LP feed-to-CP conversion using specific unit cells that convert LP to CP and CP feed-to-CP which doesn't require any conversion [73], [74]. More specifically, as shown in Fig. 11, assuming one orthogonal incident LP for the feed E^{in}, if the feed is aligned diagonally 45° to the unit

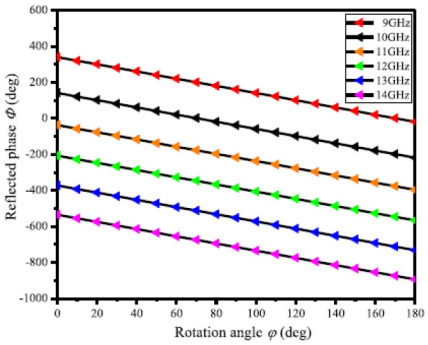

FIGURE 12. Reflection phase response versus element rotation angle [78].

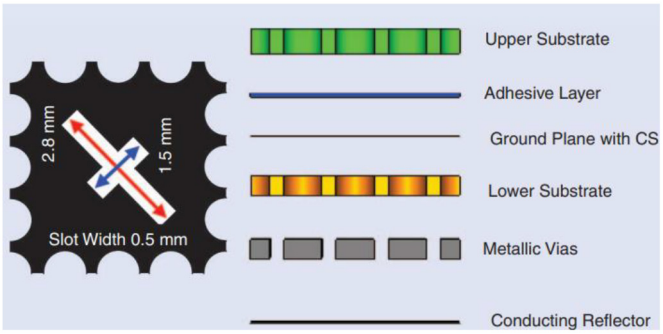

FIGURE 13. Circular Polarized RA unit cell based on rotated cross-slot [79].

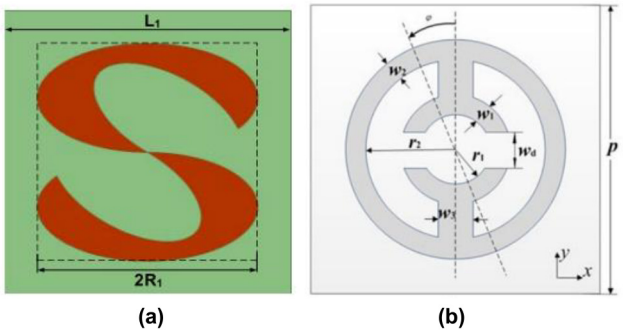

FIGURE 14. Element Angular rotation: (a) S-shaped unit cell [78] and (b) Complete and split ring [74].

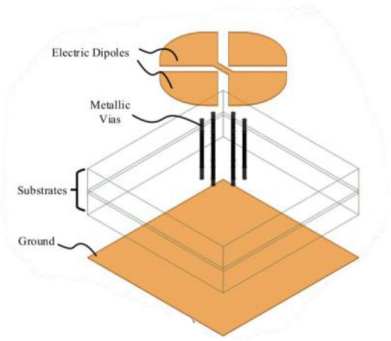

FIGURE 15. Asymmetric Magneto-Electric Dipole element [80].

cell axis, the incident wave will be decomposed into two components E_y^{in} and E_x^{in}. To achieve a CP outgoing wave E^{out}, a 90° phase difference must be introduced between the x and y components, respectively. Moreover, in the case of CP-to-CP operation, the process of designing CP RAs is inherent to Pancharatnam–Berry (PB) phase theory where the RA unit cells are rotated with different angles to obtain a co-phasal wave in the far-field by introducing a rotational dependent phase shift [39], [75].

When designing wideband CP RAs using the element rotation approach, the reflection phase response must present a linear graph in respect to the element rotation angle for different frequencies as depicted in Fig. 12. Furthermore, a wide 3-dB Axial Ratio (AR) bandwidth will ensure that the co-polarized field remains within satisfactory levels, enhancing the gain bandwidth performance of the RA. For instance, in 2013 Zhao *et al.* [76] proposed two different CP elements for a broadband CP RA and they achieved phase swing in the excess of 550° and AR and gain bandwidths higher than 30% and 40% respectively. In addition, in 2018 a quasi-I-shaped element was used as a building block by Guo *et al.* [77]. A 3dB gain bandwidth of 49.7% and a superior 3dB AR bandwidth of 75% by rotating the unit cell and maintaining the CP of the incident field using its symmetrical geometrical characteristics was achieved.

In 2017, Mahmoud *et al.* [79] proposed the use of a multilayer cross-slot unit cell which is able to achieve RHCP reflectarray radiation. As presented in Fig. 13 the unit cell is based on a multilayer configuration with a cross slot in the middle. The lengths of the two diagonal slots dictate the resonant frequency while the cross-slot rotation produces the required reflection phase of 360°. To minimize the coupling to adjacent elements, perforations are included around the unit cell and vias are used underneath the lower substrate. The unit cell was designed to reflect LHCP incident waves into RHCP radiation with a good 3-dB gain bandwidth performance of 24%.

The split ring element shown in Fig. 14 (a) and introduced by Gao *et al.* in 2018 can also be used to design CP sensitive RA unit cells which is capable of achieving wideband characteristics such as 35.8% [78]. The authors reported a reflection phase range of 400° and also highlighted the importance of using a thick substrate to suppress backscattered cross-polarization which will enhance the overall bandwidth performance. A more complex geometry was presented in 2019 by Zhang *et al.* for satellite communications [74]. More specifically, an S-shape is generated by a rotating ellipse as presented in Fig. 14 (b) has been proposed for wideband CP RAs with a reflection phase range of 350°. In this design the major axis of the ellipse was adjusted to yield cross-pol levels less than −15dB and co-pol reflection greater than −0.2dB while rotating the S-shape provided the required reflection range of 360° at different frequencies.

Recently, a novel broadband CP element was proposed in 2021 by Wu *et al.* [80] based on the Magneto-Electric (ME) Dipole. As seen in Fig. 15, the unit cell consists of two

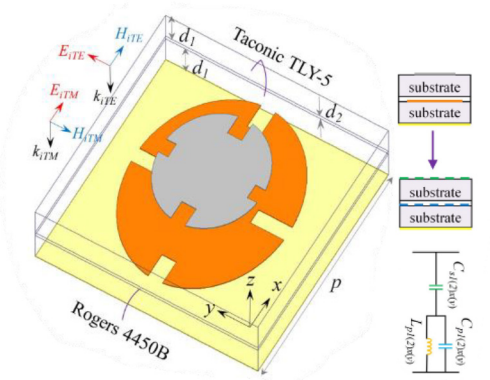

FIGURE 16. The geometry of the Ka-band dual-circular polarized elliptical slotted patch [81].

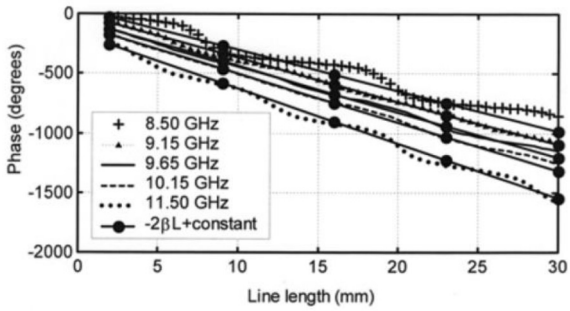

FIGURE 17. Reflection phase response versus the TTD line length [82].

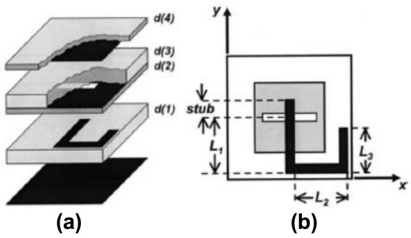

FIGURE 18. Aperture coupled to U-shaped TTD patch (a) exploded view (b) top view [82].

diagonal ME dipole pairs where each pair is responsible for each orthogonal LP polarization component. More specifically, the x-directed dipole was perturbed by connecting its opposite edges as shown in Fig. 15, to achieve a 180° phase difference between the two orthogonal LP components. This ensures that the phase of the reflected CP wave is properly controlled by rotating the element from 8-12GHz. The magnetic-dipole behavior is achieved by introducing metallic vias shorting the electric dipoles to the ground plane while the corner of the dipoles is rounded to minimize the mutual coupling variations across the aperture as the element is rotated. By rotating the unit cell from 0° to 180°, a reflection phase range of 360° was achieved with the reflection coefficient magnitude of the cross-polarized component staying below −15dB in the X-band.

Dual Polarization using the angular rotation approach was demonstrated by the authors in [81] using a unit cell based on elliptical slotted patches arranged in a 2-layer configuration as shown in Fig. 16. To achieve dual CP operation in Ka-band, the authors utilized both the Berry phase rotation and the tunable resonator approach. The authors synthesized two homogenous reactive anisotropic impedance surfaces (AIS) and computed the scattering response of each cell. By doing so, the authors claimed that a broader bandwidth can be obtained by considering the effect of the homogenized multilayer model on the reflection phase of each linear polarization. This is different from other dual CP approaches where different layers or different unit cell dimensions were responsible for each LP. More specifically, each of the two orthogonal LP incident components must be reflected with a 180° phase delay to ensure a clean co-polarized reflected wave. At the same time, the angular rotation of the unit-cell will discriminate between the two different CP waves while the lengths of the two ellipse axes will ensure an adequate reflection phase swing on each CP. In addition, slots were introduced to miniaturize the element and consequently reduce the capacitive coupling between adjacent elements of the RA. Finally, the dual CP unit cell achieved 360° reflected phased in both incident CP waves.

C. TRUE TIME OR PHASE DELAY LINES APPROACH

As stated previously, another factor that limits the bandwidth is the differential spatial phase delay introduced by different paths between the feed and the RA elements having lengths that differ in multiples of wavelength [49]. This effect is more pronounced at the edges of large reflectarrays and can be alleviated by using printed transmission lines in the element level. The technique of delay lines will introduce a physical path, providing a True Time Delay (TTD) between the incident and the reflected field [82]. This can be interpreted as a reflection phase far exceeding 360° which can reduce the phase wrap across the array aperture and minimize the phase errors due to differential spatial delays. In such designs, the reflected phase will be compared against the length of the delay line to assess the performance of the element see Fig. 17.

A popular bandwidth enhancement method using TTD lines is a multilayer structure realized using aperture coupled patch elements as shown in Fig. 18, where the open-ended stub is optimized for phase tuning. This technique was adopted in 2006 and 2008 by Constanzo *et al.* and Carrasco *et al.* respectively [82], [83] achieving a reflection phase range of 1000°. In addition, in 2008 Venneri *et al.* [84] showed that aperture coupled elements provide a bandwidth improvement from 6.7% to 17% by decreasing the inter element distance and adjusting the stub length at an operating frequency of 20 GHz. It is highlighted that the phase response of aperture coupled to TTD lines can be linear if the aperture dimensions are adjusted accordingly to cancel the resonances. Moreover, one drawback of printed delay lines is that their ohmic losses increase with increased line

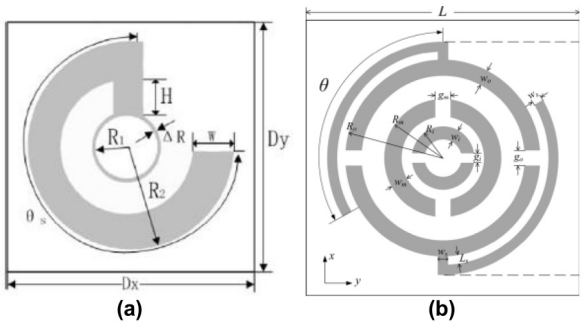

FIGURE 19. Phase delay line approach: (a) Arc phase delay line connected via a matched strip to the inner ring [86] and (b) Gapped ring with phase-delay lines [87], [88].

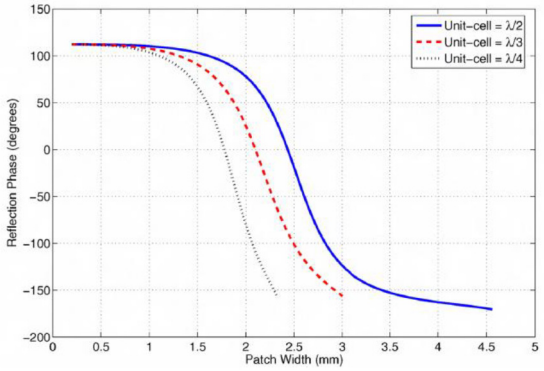

FIGURE 20. Effect of the unit cell size on the reflection phase response [94].

length, an effect that can be accounted for by employing low loss substrate material.

The concept of microstrip phase delaying elements can also be adopted in a single layer approach as seen in the work of Hasani *et al.* in 2010 and Li *et al.* in 2012 [85], [86]. Phase delay lines in a form of an arc can be used, where their length is adjusted by the angular rotation of the arc line controlling the reflection phase range of the element. There is a single ring shaped structured that is responsible for receiving the incident wave, which in turn is connected to a delay line via a matching optimized strip, see Fig. 19 (a), accounting for the travelling-to-guided wave coupling [85], [86].

Other approaches such as the work from Han *et al.* in 2019 [87], [88] involve more resonant structures packed in a single element. This includes gapped rings attached to phase delay lines as illustrated in Fig. 19 (b), resulting in an increase of the reflection phase swing over 700° and thus allowing for thicker substrates [87], [88]. Dual band designs with broad band characteristics on each band have also been reported Su *et al.* in 2019 [89], where the phase shift is adjusted individually on each frequency band by either changing the length of an arc phase delay line or the size of a ring phoenix patch for the lower and upper frequency band respectively. Low cross polarization is achieved across the array using an approach of arranging the elements in a mirror like way [90].

D. SUBWAVELENGTH PERIODICITY APPROACH

Traditional RA designs have their resonant elements arranged in a grid with $\lambda/2$ spacings whereas in the concept of subwavelength element approach, the inter-element distance is reduced to less than $\lambda/2$ while the element dimensions are kept below resonance [48]. The subwavelength design approach yields several benefits such as a reduced frequency dependent phase error, low ohmic losses, and low sensitivity to the incident angle and hence improved bandwidth. On the other hand, subwavelength periodicity presents a slightly lower gain bandwidth and reduced reflected phase range associated with strict fabrication tolerances at mm Wave frequencies as the grid resolution becomes extremely fine [50], [91], [92]. The most common subwavelength element is the rectangular patch placed in different subwavelength grids. Varying the dimensions of the subwavelength patch, the required reflection phase as well as LP to CP conversion can be obtained [93], [94].

A study by Nayeri *et al.* in 2009 [94] investigated the effect of different subwavelength unit cell sizes of square patches in the maximum reflection phase range. As illustrated in Fig. 20, one of the main difficulties in designing subwavelength unit cells is the fact that the achievable phase swing response is reduced to less than 360° when the element spacing becomes finer. This behavior is strongly associated with the coupling level which becomes weaker when the inter-element distance is reduced for small patch sizes. Reducing the grid size from $\lambda/2$ to $\lambda/3$, leads to an increase of the 0.5dB gain bandwidth from 6.25% to 9.06%.

On the other hand, in 2011 Ethier *et al.* [95] followed the approach of using square loops instead of square patches for the elements. The finding was that square loops yield an extra 50° phase swing for the same subwavelength periodicity due to their smaller electrical dimension. Around the same time in 2010 Nayeri *et al.* [92] combine the subwavelength approach in a multilayer configuration. The authors tried to achieve an adequate reflection phase range while reducing the phase error, by employing double layer subwavelength square stacked patches with $\lambda/4$ periodicity. As a result, the bandwidth is increased by more than 80% of its $\lambda/2$ counterpart. Moreover, a slight increase in the antenna gain by 0.1dB was also observed due to the inherent lower reflection loss of the double layer architectures.

Later in 2015, Qin *et al.* [96] presented a $\lambda/5$ unit cell composed of two square loops with meandering as depicted in Fig. 21 (a). The meander lines allow the subwavelength element to achieve a 420° reflection phase range by varying their length. This is an increase of 120° as compared to simple square loops with $\lambda/5$ periodicity. More recently, in 2018, Mohammadi *et al.* [97] attempted to reduce the sensitivity of the reflection phase by using concentric rings elements. As shown in Fig. 21 (b), the unit cell is composed of rings with variable widths at $\lambda/3$ periodicity. A phase constant in the aperture phase distribution was used to obtain

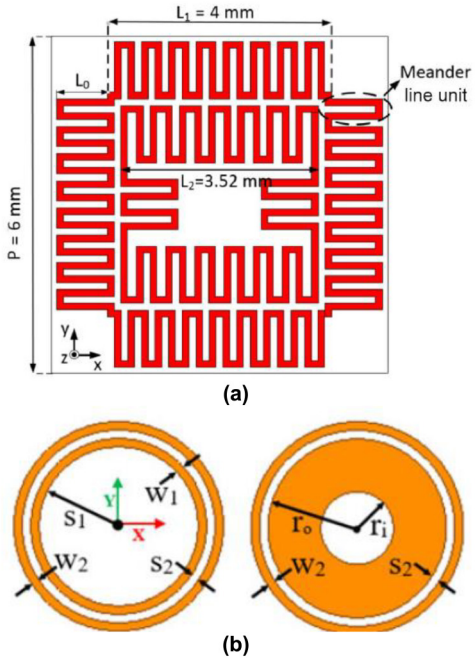

FIGURE 21. Subwavelength unit cells: (a) square loops with meandering [96] and (b) concentric rings [97].

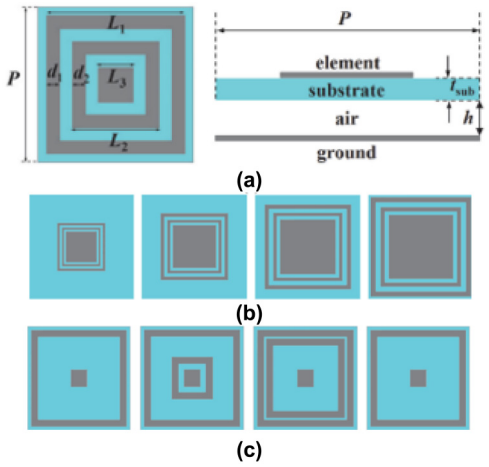

FIGURE 22. Dual band RA using the hybrid design approach (a) top and side view, (b) multi-resonant element and (c) Phoenix element [100].

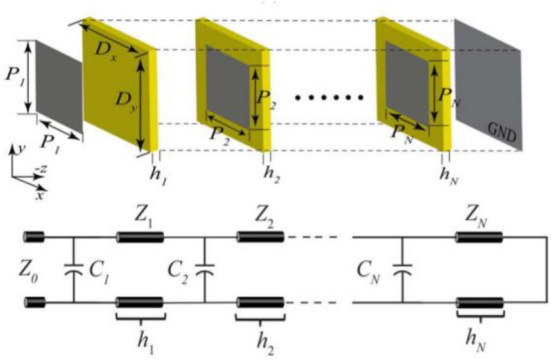

FIGURE 23. Unit Cell based on the MEFSS and the equivalent circuit [101].

reduced reflection phase sensitivity and achieve linear 423° phase response allowing the use of thicker substrates.

One of the modeling limitations of reflectarrays which is the assumption of identical unit cells to approximate an infinite periodic structure was investigated in 2014 by Ethier *et al.* [98]. They stressed out the fact that if the geometrical features of adjacent elements differ a lot, then significant radiation pattern degradation can be observed. They developed a new technique to synthesize apertures with unit cells that are optimized for geometrical similarity based on the concept of fragmented elements providing a reflection phase range of 300°. A combination of subwavelength periodicity and phase delay lines was introduced by Yu and Guo in 2019 [99]. A subwavelength element that has integrated variable length phase delay lines in the form of sectorial slits was designed achieving a reflected phase range of 300°. The element periodicity was chosen at $\lambda/3$ while the sectorial slits provided the required phase delay keeping the mutual coupling between adjacent cells identical.

Another hybrid technique to design a wideband reflectarray based on the subwavelength spacing, multi-resonant and multitype structures and dual frequency synthesis is suggested by Deng *et al.* in 2017 [100]. The multi-functional unit cell is based on the phoenix design presented in [51] by Mustafa *et al.* in 2011 and is proposed for Ku-band satellite communications, see Fig. 22. Two different unit-cell types are used, namely the double square loops with inner square patch and the Phoenix element, as shown in Fig. 22 (b) and (c), respectively. Moreover, both of the element types are used to jointly provide the required reflection phase in both frequencies (e.g., 12.5 and 14.25GHz). Despite the subwavelength periodicity, the unit cell achieved a full 360° reflection phase range which is mainly attributed to the rebirth capability of the phoenix element.

A combination of subwavelength periodicity and TTD unit cell have been presented in 2015 by Abadi *et al.* [101]. The unit cell is based on non-resonant capacitive patches and follows the concept of Miniaturize-Element-Frequency-Selective-Surfaces (MEFSSs). The patches are arranged in a multilayer configuration, as shown in Fig. 23, and are modelled as parallel capacitors while the dielectric layers are considered as transmission lines. The phase response of the TTD unit cell can be visualized as lowpass MEFSS filter. To obtain a constant group delay, the reflected phase response versus frequency must be linear. In addition, the number of patch layers is proportional to the maximum delay variations that can be provided by the MEFSS. Hence, by increasing the number of layers, the RA bandwidth can be increased accordingly. In [101], the authors used two patch layers and a 0.22λ grid periodicity as the TTD unit cell. The side of the square patches was varied accordingly to control the required delay or phase shift across the aperture. This allowed for a maximum delay of 160ps for the center unit cells and a highly linear reflection phase response with

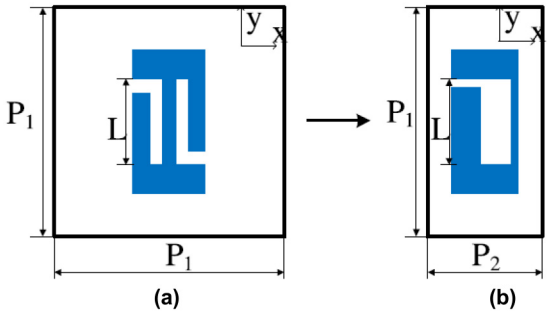

FIGURE 24. Half-cut unit cell evolution (a) original geometry [103] and (b) half-cut geometry [102].

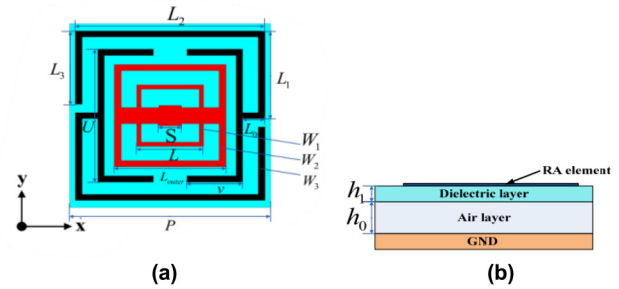

FIGURE 25. Square split ring with delay lines and phoenix dual band unit cell (a) top view and (b) side view [70].

a maximum of 500°. Finally, the authors emphasized on the suitability of the aforementioned MEFSS unit cell for X-band broadband pulsed applications with insignificant chromatic deviations over the frequency band of interest.

Lately, in 2021 Ning *et al.* [102] applied a well-known antenna miniaturization technique called half-cut approach on a subwavelength unit cell proposed in 2019 by Guo *et al.* [103]. As shown in Fig. 24, the original geometry is based on a $0.3\lambda \times 0.3\lambda$ rectangular with two inverted L-slots while the half-cut geometry has size of $0.15\lambda \times 0.3\lambda$ is using a single L-slot. In both designs, the length of the slot is varied across the y-direction to obtain a linear reflected phase response of around 330° insensitive to frequency variations between 9-12GHz. Even though the half-cut unit cell has smaller size, the achievable phase range is maintained. The reason is that only the dimension across the x-direction was halved. Moreover, it is important to mention that the outer dimensions of the rectangular patch remain constant across the aperture as opposed to conventional unit cells. This results in equal mutual coupling between neighboring unit cells of the RA. By using the half-cut technique, the number of RA elements was doubled from 529 to 1058 at X-band. This contributed to a 9% increase in the 1-dB gain bandwidth over the original geometry.

A way to achieve wide bandwidth and dual polarization capability when the RA operates in two different frequencies was proposed by [70]. The unit cell consists of two different element types, namely a square split ring with delay lines which is responsible for the X-band and a square phoenix

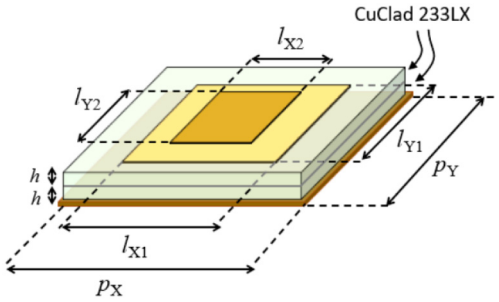

FIGURE 26. Dual layer unit cell based on stacked rectangular patches for LP-to-CP conversion [104].

cell for the K-band as seen in Fig. 25. Moreover, the unit cell operates in to two different bands and in each band presents two different orthogonal polarizations, hence reducing the mutual coupling between the two polarizations in the X and K-band. The reflection phase can be controlled independently in each frequency bands by controlling the phase delay lines in X-band and the dimensions of the inner square phoenix cell in K-band. A subwavelength grid periodicity was used in the X-band of 0.3λ at 10GHz while 0.66λ was adopted for the higher frequency of 22 GHz. Furthermore, an air gap was used between the dielectric layer and the ground plane to smooth the reflection phase response of the unit cell and achieve a 360° phase response in both frequencies and polarizations.

Rectangular stacked patches have also been employed as unit cells to design dual CP RAs as presented by [104]. The unit cell is shown in Fig. 26 and follows a 2-layer configuration operating in 20 GHz. A proportion of 0.8 between the lengths of the top and bottom patch was kept in order to generate two close resonances providing a larger reflection phase range. Each unit cell independently controls the phase shifts of the x and y components of the incident field. More specifically, by varying the dimensions of the patch along the x-direction and across the y-direction the reflection phase of the x and y components of the incident field can be controlled respectively. In addition, the phase shift distributions of the x and y components must be 90° out of phase to generate a CP reflected beam. To enhance the bandwidth, the unit cell presents a periodicity of $0.4\lambda \times 0.4\lambda$ at 20 GHz achieving a reflected phase close to 500° for both the x and y component of the incident field.

Another type of unit-cell that offers polarization diversity is based on the Jerusalem Cross (JC) which it can be seen as crosses with capacitive loading as depicted in Fig. 27. The first dual CP reflectarray using a dual LP feed is reported in [73]. The 400 element X-band reflectarray was able to operate on dual CP mode while using a dual LP feed by utilizing the polarization conversion concept shown in Fig. 11. The unit cell achieved 400° reflection phase for both x and y directed length variations of the cross. In addition, the effect of the y-directed geometric variations on the x-directed reflected phase response were investigated. The maximum

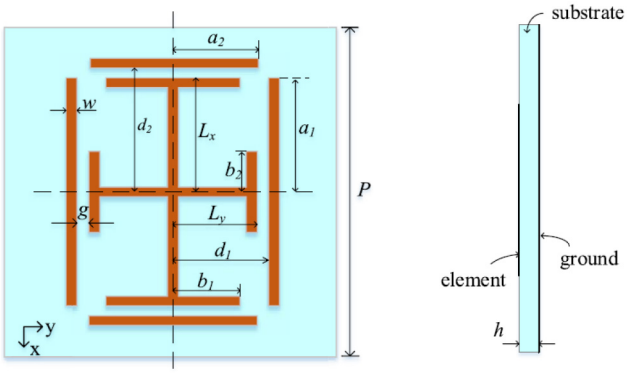

FIGURE 27. Jerusalem cross dual CP unit cell [73].

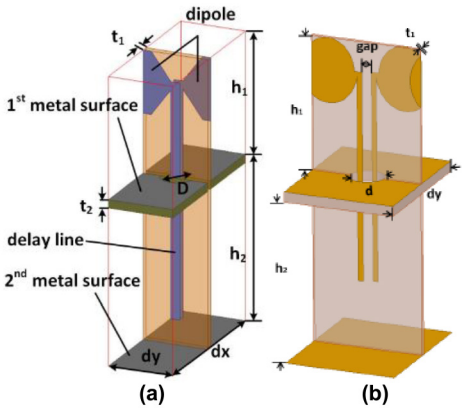

FIGURE 28. Tightly coupled unit cells: (a) Bowtie printed dipole [105] and (b) Elliptical printed dipole with variant coupling capacitance [107].

phase variation was found to be 20° indicating low mutual coupling between the two orthogonal polarizations.

Furthermore, a technique that is closely related to the subwavelength periodicity and the mutual coupling between the elements is known as tightly coupled reflectarrays. In 2018 Li *et al.* [105] introduced the concept of tightly coupled RAs. This concept is based on the ultra-wideband operating characteristics of connected arrays and tightly coupled antenna arrays to enhance the bandwidth performance. Tightly coupled and connected arrays operation is based on the mutual coupling between the elements which can be achieved by placing the antenna elements close to each other or by using inductors and capacitors between elements to increase their electromagnetic interaction [106].

In conventional RAs, the inter-element distance is half the wavelength of the operating frequency while in the tightly coupled RA reported in [105], the distance is reduced to $\lambda/10$ of the wavelength of the lowest operating frequency. The authors used tightly coupled printed dipoles mounted perpendicularly through two metallic surfaces, see Fig. 28 (a). The phase tuning technique was the guided wave approach. More specifically, the printed bowtie dipole was coupled to at true time delay line to account for the spatial phase delay induced by the distance between the feed antenna and the reflective surface. The height of the delay line was chosen to tune the phase of the reflected wave accordingly.

The work of tightly coupled RAs was extended recently by Wang *et al.* in 2020 [107]. As depicted in Fig. 28 (b), an RA with improved aperture efficiency is achieved by utilizing the variant-coupling capacitance and true time delay line methods. The element is based on an elliptical printed dipole and in the case of [107] overlapping of the adjacent elements is allowed which is explained as variant coupling capacitance. Therefore, the coupling capacitance along with the length of the time delay lines are taken into consideration when designing the unit cell that achieves a reflection phase range of approximately 500°.

IV. WIDEBAND REFLECTARRAY SYSTEM ANALYSIS

As outlined in Section III, the bandwidth of the reflectarray system is mainly limited by the choice of unit cell and the available reflection phase range. However, other metrics contribute to the overall gain bandwidth of the RA such as the size of the aperture, the Focal Length (F/D) of the feeding system and the choice of the substrate material and structure.

When considering the full reflectarray system, according to the choice of the wideband design approach, a balance must be kept between gain bandwidth performance, cost, and system complexity. Hence, in this section, the tradeoffs of each wideband design approach will be investigated from an RA system perspective. More specifically, existing wideband RA implementations are categorized in Table 2 according to their wideband techniques and are critically analyzed in terms of the side lobe levels (SLLs), cross-polarization levels (X-pol), feed focal distance (also known as F/D ratio), aperture efficiency (AE), maximum gain, 1-dB gain bandwidth, reflectarray size, substrate, polarization, and operating frequency band. The reflection phase range and the type of unit cell, which were investigated in the Section III, are also considered in the full RA system analysis. In Section IV-A, a critical analysis of the RA system performance metrics is provided. rather than a comparative one since the RA designs in Table 2 are grouped according to different wideband techniques rather than operating frequencies.

Following this, in Sections IV-B–IV-E the different approaches are assessed from an RA system perspective and finally in Section IV-F the approaches are compared against each other. The performance comparison is implemented according to the following strategy: Wideband RA designs operating at the same frequency band and using the same wideband phase tuning approach are compared in Sections IV-B–IV-E; Wideband RA designs operating at different frequency bands and using the different wideband phase tuning approaches are compared in Section IV-F. Therefore, the aim of the following presented analysis is to evaluate the performance of the different wideband phase tuning approaches as well as to compare the different approaches with an insight into the full RA system.

TABLE 2. Wideband reflectarrays categorized according to the approach used.

Approach		Design	F/D	Cross Pol [dB]	Peak SLL [dB]	AE%	Max Gain [dBi]	1-dB Gain 3-dB AR (for CP) BW %	RA size [mm^2]	Substrate Profile [mm]	Pol	Reflection Phase Range [degrees]	Frequency
Multi Resonance	Single Layer	Three Parasitic Dipoles [59]	-	-	-	-	14.2@2.1GHz (directivity)	14.1*	660x300 $4.6\lambda_0 * 2\lambda_0$	h=0.76 ε_r=2.5	LP	528	S-band 1.95-2.15
		Five Dipoles [60]	1.42	-30	-15.4	64.1	31.4@15GHz	33.52	300 Diameter $15\lambda_0$	h=3.175 ε_r=2.2	LP	800	Ku -band 13.87-19.68
		Concentric Square and Cross Shaped Loops [62]	0.8	-22	-20	50	40.6@12GHz	12	1200x1200 $48\lambda_0 * 48\lambda_0$	h=3.175 ε_r=2.17	LP	500	Ku-band 11.4-12.8 13.7-14.5
		Sloted Patch Concave Arms [61]	0.71	-32	-20	65	25.7@10GHz	32	207x207 $6.9\lambda_0 * 6.9\lambda_0$	h=3.175 ε_r=2.2	LP	360	X -band 10.5-14.1
		Dual Resonance Square Patch [54]	1.3	-	-20.4	47	31.9@45GHz	29.3	108x108 $18\lambda_0 * 18\lambda_0$	h=0.508 ε_r=2.2 Air-1mm	LP	360	Q-band 42.3-48.4
		Double Split Ring with I-shaped dipole [63]	2.35	-25	-	50	26.6@13GHz	22.7*	200x200 $8.7\lambda_0 * 8.7\lambda_0$	h=1.5	LP	360	Ku-band 11.6-14.6
		I-shaped dipole [64]	-	-15	-10	38.5	15.5@10.5GHz (directivity)	22.3*	100x60 $3.5\lambda_0 * 2\lambda_0$	h=1.5 ε_r=2.2	LP	400	X-band 9.5-12

(continued.)

IEEE Open Journal of Antennas and Propagation

TABLE 2. *(Continued.)* **Wideband reflectarrays categorized according to the approach used.**

		Malta Cross [58]	1.78	-	-	62	33.5@11.7GHz	19	411x411 $16\lambda_0 * 16\lambda_0$	h=1.6 ε_r=3	LP	-	X-band 11.2-12.2
		Archimedean Spiral [65]	1	-27.5	-20	60.2	28.3 @13.58GHz	28.7	220x220 $10\lambda_0 * 10\lambda_0$	h=3 ε_r=2.2	LP	540	Ku-band 12.41-16.31
		Spline [21]	1.06	-19.2	-15.1	64.7	25@10GHz	37	210x210 $7\lambda_0 * 7\lambda_0$	h=1.57 ε_r=2.33 h=3 Air	LP	450	X-band 8.85-12.85
		Spiral Dipole with Square Ring [66]	0.77	-30	-14	55	26.5@8GHz	35	300x300 $8\lambda_0 * 8\lambda_0$	h=2 ε_r=2.2	LP	360	X-band 6.6-9.4
	Multilayer	**Two-layer T-shaped Patch [57]**	1	-28	-15	44	19.4@9.5GHz	20 28 (3-dB AR)	126x126 $4\lambda_0 * 4\lambda_0$	h1=2 h2=2 ε_r=2.65	CP	400	X-band 8.5-11.5
		Three-layer Square Patch [55]	0.85	-	-	-	-	10	1050x994 Elliptical $42\lambda_0 * 39.6\lambda_0$	h1=3 h2=3 h3=3 Honeycomb	LP	800	Ku-band 11.7-12.6

(continued.)

TABLE 2. *(Continued.)* **Wideband reflectarrays categorized according to the approach used.**

		Two-layer Square Patch [44]	0.83	-25	-30	-	31@12GHz	16.7	406x406 $16.2\lambda_0 * 16.2\lambda_0$	h=2 ROHACELL 51 h=2 ROHACELL 51	LP	400	Ku-band 11-13
		Parallel Stacked Dipoles [69]	0.89 0.98	-23.82 -26.18	-13.65 -8.47	-	27@12GHz 28@19.5GHz	20^ 5^	250x250 $10\lambda_0 * 10\lambda_0$ $16.23\lambda_0 * 13.23\lambda_0$	h1=2.363 ε_r=2.55 h2=1.5 ε_r=2.17	Dual LP in each frequency band	400 500	Ku/K-band 11-13 19-20
		Lateral Stacked Dipoles [19]	1.4	-28	-20	77	28@11.3GHz 34@14GHz	27^	454 Diameter $17.1\lambda_0$	h1=2.363 ε_r=2.55 h2=1.5 ε_r=2.17	Dual LP	720	Ku-band 11.24-14.25
Element Rotation		**Double Split Ring I-shaped Dipole [76]**	1	-25	-20	59.9	25@9.9GHz	30 43 (3dB AR)	195x195 $6.5\lambda_0 * 6.5\lambda_0$	h=1.5 ε_r=4.4 h=2.2 Foam	CP	550	X-band 9.2-12.4
		Double Layer Cross Slot [79]	0.7	-25	-17.5	-	25@30GHz	24* 26 (3dB AR)	90x90 $9\lambda_0 * 9\lambda_0$	h1=0.635 ε_r=10.2 h1=0.508 ε_r=2.2	CP	360	Ka-band 27-35
		Complete ring and Split Ring Resonator [78]	0.7	-22	-20	52.3	24dBic@14GHz	35.8 25.8 (3-dB AR)	119x119 $4.76\lambda_0 * 4.76\lambda_0$	h=3.175 ε_r=2.2	CP	400	Ku-band 9-15

(continued.)

TABLE 2. *(Continued.)* **Wideband reflectarrays categorized according to the approach used.**

	S-shaped Rotational [74]	0.97	-15	-15	60	25.2dBic@11.6 GHz	47.8* 68.5 (3-dB AR)	180x180 $7\lambda_0 * 7\lambda_0$	h=0.5 ε_r=3.55 h=4 air	CP	350	X -band 8.6-14
	Quasi I-shaped [77]	0.88	-20	-20	58.6	30@16GHz	33.6 75 (3-dB AR)	215x215 $11.4\lambda_0 * 11.4\lambda_0$	h=2.5 ε_r=2.9	CP	500	Ku -band 12.4-20.6
	Magneto Electric Dipole [80]	1.2	-20	-18	60	24dBic@11GHz	41* 42 (3-dB AR)	176x176 $6.45\lambda_0 * 6.45\lambda_0$	h=3 ε_r=3.66	CP	360	X-band 8.2-12.4
	Elliptical Slotted Patch [81]	0.92	-32	-19	43.4	30.2dBic@30GHz	31.5 29.5 (0.5-dB AR)	156 Diameter $15.6\lambda_0$	h2=0.254 ε_r=2.2 h2=0.254 ε_r=3.52	Dual CP	360	Ka-band 26-38GHz
True Time or Phase Delay Lines	**Aperture Coupled to U-shaped TTD [82]**	0.94	-15	-20	60	36.3@9.65GHz	26.7**	840 Diameter $27\lambda_0$	h1=0.5 ε_r=1.06 h2=2 ε_r=3.38 h3=0.5 ε_r=1.06 h4=7.7 ε_r=3.38	LP	1000	X -band 8.5-11.9
	Aperture Coupled to I-shaped TTD [84]	1	-	-	-	-	17	187 Diameter $12.8\lambda_0$	h1=0.762 ε_r=2.33 h2=0.762 ε_r=2.33 h3=3.7 Air	LP	190	K-band 18.8-22.2

(continued.)

TABLE 2. *(Continued.)* **Wideband reflectarrays categorized according to the approach used.**

	Disk with circular phase delay line [85]	Center fed low efficiency	-13	-15	35	24@11.7GHz	18*	190x270 $7.4\lambda_0 * 10.5\lambda_0$	h=0.83 ε_r=3.38	LP	450	X-band 10.7-12.7
	Ring with open-circuited stub [86]	1	-	-15	52	24.9@11.5GHz	17.8*	195x195 $7.5\lambda_0 * 7.5\lambda_0$	h1=0.5 ε_r=2.2 h2=3.175 Foam	LP	450	X -band 10.95-13
	Gapped Rings With Phase Delay Lines [87, 88]	0.77	-26	-20	50	25.78@10GHz	31.5	266 Octagon Diameter $8.8\lambda_0$	h1=0.8 ε_r=3.55 h2=2 air	LP	600	X -band 9.7-13.33
	Split Ring with Phoenix Patch [89]	1.3	-26 -30	-15 -14	40 44.8	22.9@8.5GHz 28.8@16GHz	20.7 12.9	225x225 $6.37\lambda_0 * 6.37\lambda_0$ $12\lambda_0 * 12\lambda_0$	h1=1 ε_r=3.5 h2=2 air	LP	550 (X-band) 360(Ku-band)	X/Ku-band 7.9-9.7 14.7-16.8
Subwavelength Periodicity	**Sub wavelength $\frac{\lambda}{3}$ square patch [94]**	1	-	-	-	29.10@32GHz	9.06 ****	139.5x139.5 $15\lambda_0 * 15\lambda_0$	h=2 ε_r=2.2	LP	260	Ka-band 30.3-33.2
	Double layer sub wavelength $\frac{\lambda}{4}$ square patch [92]	0.61	-	-	-	32.55@32GHz	19.13	159 Diameter $16.96\lambda_0$	h1=n/a ε_r=2.2 h2=n/a ε_r=2.2	-	277	Ka-band 30.07-36.43
	Sub wavelength $\frac{\lambda}{3}$ rectangular patch [93]	1	-22	-14	39	25.8@10GHz	17 11 (3-dB AR)	270x270 $9\lambda_0 * 9\lambda_0$	h=2 ε_r=2.65	CP	300	X-band 9.2-10.9

(continued.)

IEEE Open Journal of Antennas and Propagation

TABLE 2. *(Continued.)* **Wideband reflectarrays categorized according to the approach used.**

	Sub wavelength $\frac{\lambda}{6}$ square loop [95, 108]	-	-	-	-	32@13GHz	18.5	400x400 $17.4\lambda_0 * 17.4\lambda_0$	h=1.54 ε_r=4.45	LP	309	Ku-band 12-14.5
	$\frac{\lambda}{5}$ Square Loops With Meander Lines [96]	1	-30	-20	56.5	28.2@10.1GHz	18**	288x288 $9.6\lambda_0 * 9.6\lambda_0$	h=3.75 ε_r=2.2	LP	370	X-band 9-11
	$\frac{\lambda}{3}$ Concentric Rings [97]	1.1	-31.7	-20.7	44.56	26.6@10.2GHz	23.3	300 Diameter $10.2\lambda_0$	h1=0.813 ε_r=3.55 h2=1.524 ε_r=4.4	-	423	X-band 9.57-11.2
	$\frac{\lambda}{6}$ Similarity-Shaped Fragmented Elements [98]	1.09	-28.8	-20.6	97.4	33.06@11.2GHz	12.3	420x420 $15.7\lambda_0 * 15.7\lambda_0$	h1=0.127 ε_r=4.4 h2=4 *Foam*	-	300	X -band 10-13.5
	$\frac{\lambda}{3}$ Circular Ring with Slits [99]	0.71	-32	-17.5	58.3	25@10GHz	30	207x207 $6.9\lambda_0 * 6.9\lambda_0$	h=3.75 ε_r=2.2	LP	350	X -band 8-16
	$\frac{\lambda}{3}$ Hybrid Phoenix Element [100]	0.9	-26	-20	70 69	32.8@12.5GHz 33.9@14.25GHz	29 for AE 40%	400 $16.6\lambda_0$ $19\lambda_0$	h1=0.79 ε_r=2.55 h2=4 *Air*	LP	360	Ku-band 12.25-12.75 14-14.5
	$\frac{\lambda}{5}$ Miniaturized Element FSS [101]	0.8	-20	-10	-	23@10GHz	40*	253.5x253.5 $8.5\lambda_0 * 8.5\lambda_0$	h1=1.524 ε_r=3.4 h2=0.1 ε_r=3.52 h1=1.524 ε_r=3.4 h2=0.1 ε_r=3.52 h1=1.524 ε_r=3.4	LP	-	X-band 8-12

(continued.)

TABLE 2. *(Continued.)* **Wideband reflectarrays categorized according to the approach used.**

	$\frac{\lambda}{3}\times\frac{\lambda}{6}$ **Half-cut L-slotted Rectangular Patch [102]**	0.71	-30	-17	62.7	26@10GHz	31	207x207 $6.9\lambda_0 * 6.9\lambda_0$	h=3 ε_r=2.2	LP	330	X-band 9-12
	Square split ring with delay lines (X-band) Square phoenix cell (K-band) [70]	1.2 1	-30 -50	-15 -19	48 43	23.6@10GHz 30.6@22GHz	20 19	200x200 $6.6\lambda_0 * 6.6\lambda_0$ $14.7\lambda_0 * 14.7\lambda_0$	h1=1 ε_r=3.5 h2=2 Air	Dual-LP X-Pol in K-band Y-Pol in the X-band	360	X/K-band 9-11 20-24
	Stacked Rectangular Patch [104]	-	-26	-16	57.3 LHCP 52.7 RHCP	29.95@19.7GHz	20 19 (3-dB AR)	180x180 $12\lambda_0 * 12\lambda_0$	h2=0.787 ε_r=2.33 h2=0.787 ε_r=2.33	Dual CP	500	K-band 17.2-22.7
	$\frac{\lambda}{3}$ **Jerusalem Cross [73]**	0.84	-25	-27	46.3	24.4@12.5GHz	12.5 50 (3-dB AR)	166x166 $6.6\lambda_0 * 6.6\lambda_0$	h=3 ε_r=2.2	Dual CP	400	X-band 11-13
	Tightly Coupled Bowtie Printed Dipole [105]	0.56	-20	-11.7	38	22.6@10.6GHz	31.2***	210x210 $7.4\lambda_0 * 7.4\lambda_0$	h1=0.81 ε_r=3.55 h2=3.1 *Air*	-	-	X-band 3.4-10
	Tightly Coupled Elliptical Printed Dipole with Capacitive Variant Coupling [107]	1	-20	-	47.5	21.9@5GHz	25***	350x350 $5.8\lambda_0 * 5.8\lambda_0$	h1=1 ε_r=3.55 h2=17.9 *Air*	-	500	C-band 2-5

* 3-dB gain Bandwidth, ** 1.5-dB gain Bandwidth, ***-10-dB Impedance Bandwidth, **** 0.5-dB gain Bandwidth,^ 2-dB gain Bandwidth

IEEE Open Journal of Antennas and Propagation

A. SYSTEM PERFROMANCE METRICS

1) GAIN BANDWIDTH

In Table 2, the RA gain bandwidths are expressed either as 3-dB, 1.5dB and the most common one being 1-dB. This metric gives an insight into the operating frequency range where the RA can maintain a good gain performance which is vital for 5G/6G applications. A performance baseline for the gain bandwidth of RA is 10% where bandwidths higher than this value are considered to be wideband [48], [49]. In the investigated literature on wideband RAs, the reported gain bandwidths range from 9.06% up to 37% for 1-dB and up to 49.7% for 1.5dB. The gain bandwidth depends on several factors such as the unit cell available reflection phase range, the F/D, the substrate thickness and the corresponding phase tuning approach. Apart from that, the system performance in terms of SLLs and Cross Pol levels can give an additional level of information into the gain bandwidth performance of the RA system.

2) FREQUENCY AND SUBSTRATE

As shown by the designs presented in Table 2, the focus area of wideband RA research ranges from the X-band up to Ka-band with most works being in X-band and a few reported designs in the L, S and C-bands. In terms of dielectric materials all the designs utilize dielectrics with constants ranging from 10.5 down to 2.2 with most of them showing a preference to low loss materials of 2.2. In addition, many of the reported designs have an extra layer of air, foam, honeycomb or ROHACELL51 to increase the linearity of the reflection phase curve. However, thicker substrates decrease the achievable reflection phase swing. This in turn leads to phase errors across the aperture which translates to gain bandwidth degradation as indicated by the authors of [94] with a 260° reflection phase range and a 1-dB gain bandwidth of less than 10%. To account for this fact, several wideband RAs presented in Table 2 provide reflection phase ranges in the excess of 360°, [55], [60], [87], [88] with the maximum reflection phase reaching 1000° and corresponding to the in TTD approach [82].

3) POLARIZATION, DUAL POLARIZATION AND AXIAL RATIO BANDWIDTH

Furthermore, the choice of the antenna polarization is another important design aspect for wideband RAs and highly correlated with the adopted wideband approach. More specifically, most of the wideband design studies investigate LP RA using the multi resonance, TTD and subwavelength approaches with the exemption of the element rotation approach which is inherent to CP RAs. For CP RAs, the 3-dB Axial Ratio (AR) bandwidth must be considered along with the gain bandwidth. The effective operating range of the RA would be the intersection of the gain bandwidth and the AR bandwidth ensuring that the RA can maintain a satisfactory gain as well as polarization purity. The AR bandwidths presented in the wideband designs of Table 2 [57], [74], [76], [77], [78] and [79] range from 11 up to 75% and in most of the cases are larger than the corresponding gain bandwidths.

Dual polarized reflectarray operation requires dual polarized incident waves. This can be accomplished by using either dual CP or dual LP feed systems. The simplest approach would be to use a dual LP feed or dual CP feed to achieve either dual LP or dual CP radiation from the RA aperture. Among the two design choices, the complexity in designing and fabricating dual CP feeds is higher as compared to dual LP ones [73]. However, dual CP operation can be achieved by using a dual LP feed oriented 45° diagonally to the unit cell axis as indicated by [73] and [104]. To achieve dual LP using a dual LP feed in a single frequency band, the RA element geometry needs to handle simultaneously the phase delay across the x-and the y-direction controlling X- and Y-polarized reflection in the same frequency band, respectively. This poses challenges in reducing the in band cross-polarization levels as indicated by the works in [19], [69], [71]. The most popular unit cell geometry is the printed stacked dipoles as it offers 6 degrees of freedom per unit cell. The design in [71] presents the lowest cross-polarization levels of -37 dB among the dual polarized designs in Table 2 which highlights the importance of using optimization routines for cross-polarization reduction in dual polarized single band RAs. Other approaches have been proposed where two different unit cells are employed in a single layer RA with one controlling the X-polarized reflection and the other the Y-polarized reflection as in the case of fractal patches [29]. The main difference with the printed stacked dipoles is that it reduces the complexity and manufacturing cost by using only one functional layer. However, the gain bandwidth performance is deteriorated to as low as 2.4%.

In the case of dual CP operation from a dual CP feed in a single band a $+90°$ or $-90°$ phase difference must be introduced across the x- and y-direction corresponding to LHCP and RHCP respectively [90]. This must be achieved by purely varying the geometrical parameters of the unit cell arranged in a 2-layer configuration. Different layers can be used to handle different polarizations where each layer accommodates the same [81] or different unit cell families [109]. The design in [81] outperforms the dual CP in a single band designs in Table 2 with an AE of 41% and an exceptional 1-dB gain bandwidth of 31.5%.

To achieve dual polarization with each orthogonal polarization in different frequency band, two separate feeds, a dual band, or a broadband feed with either dual or single polarization on each band can be used. The most common technique is to design unit cells that contain two different families or element shapes where each shape corresponds to a different frequency band [70]. Each element family within the unit cell then controls a polarization in a single frequency band. This polarization is orthogonal or has opposite handedness to the polarization in the other frequency band. Hence the cross-polarization requirements of these type of RAs are easier to be satisfied as shown by the designs

in [70], [110] and [111] where the cross-polarization levels are kept below −20dB. However, the drawback of the dual band polarization diversity is that the gain bandwidth must be studied and optimized in two frequency band simultaneously, as indicated by [110] with a low 1-dB gain bandwidth of 5% on each frequency band.

4) FEEDING SYSTEM AND APERTURE SHAPE

The study of the feeding system is a vital and an initial step in the RA design in order to maximize the illumination efficiency and reduce the spillover losses. To do that, the F/D of the feed must be selected so that a −10dB edge taper is applied to the reflectarray. The feed type, location and aperture size will determine the final illumination and spillover efficiency which contribute to the aperture efficiency (AE). In terms of feeding systems, the F/D ratios vary from 0.61 up to 2.35, while the most common F/D is close to 1. Keeping a high F/D value, meaning the feed is placed further away from the aperture, ensures that the plane wave and point source approximations used during the design of the RA are more accurate. Accordingly, the feed position in all of the RA systems are offset configurations apart from the design in [85] and [101]. Moreover, the AEs in Table 2 range from 35 to 97% which are also strongly related to any phase errors or unwanted cross-polarizations. The size and shape of the RA aperture is mainly decided on two factors, namely the feed system design and the required directivity of the RA system. From the wideband RAs listed in Table 2, we can see that 4 different shapes are identified. More specifically, there are circular, rectangular, square, and elliptical apertures. These apertures come in a variety of sizes ranging from $2\lambda_0$ up to $50\lambda_0$ for small and large RAs, respectively. A direct consequence to the aperture size and AE is the maximum gain of the RA. The reported gains range from 14.2dBi for a small sized RA of $4.6\lambda_0 * 2\lambda_0$ [59] up to 40.6dBi that corresponds to one of the largest wideband RAs with aperture size of $48\lambda_0 * 48\lambda_0$ [62], see Table 2.

B. MULTI-RESONANCE APPROACH EVALUATION

From the investigated literature, 16 wideband RAs use the multi resonance approach either in a single or multilayer configuration. The designs operated either in S, X, Ku, and Q-band frequency range.

The designs operating in X-band are presented in [21], [57], [58], [61], [64], [66]. Among these designs, the one in [21] achieved a gain of 25 dBi at 10 GHz and presents the highest 1-dB gain bandwidth of 37%. This can be attributed to two factors. Firstly, the inclusion of a 3 mm air gap underneath the unit cell and secondly the unit cell geometry design technique which is based on a CGA and the spline technique. The design on [66] achieved the second highest 1-dB gain bandwidth of 35% but using only a single substrate layer. Instead of using air as an additional layer to smoothen the reflection phase response, the authors of [66] incorporated 4 square ring in the unit cell. Moreover, to reduce the phase errors across the aperture between actual and expected values, two degrees of freedom were used. This resulted in a maximum phase deviation of 20° in the design frequency of 6.5GHz. A comparable performance is observed in the work of [61] which provides a 1-dB gain bandwidth of 32% without using an additional air layer. As a result, the aperture profile is reduced from 4.57mm in [21] to 3.175mm in [61]. Both [21] and [61] have a comparable aperture size of $7\lambda_0 * 7\lambda_0$ and $6.9\lambda_0 * 6.9\lambda_0$ at 10GHz and F/D of 1.04 and 0.71, respectively. A noticeable difference between the two designs is the cross-polarization performance. The design in [61] presents exceptional cross polarization reduction of −32dB as the elements are arranged in a mirror symmetrical way. This technique ensures that the current cross polar components of adjacent elements are directed in opposite directions, hence they destructively interfere in the far-filed greatly reducing the cross polarized radiation [112]. An observation among the multi resonance X-band designs of Table 2 is that when the aperture size is increased, which is the case in [58] with a size is $16\lambda_0 * 16\lambda_0$, the 1-dB gain bandwidth deteriorates to 19%. A larger aperture size yields higher gain, but it introduces spatial phase delay and as a consequence the bandwidth is decreased.

The designs reported in [19], [44], [55], [60], [62], [63], [65], [69] operate in the Ku/K-band. From these works, the highest gain bandwidth performance is observed in [60]. Even though this is a $15\lambda_0$ circular RA at 15GHz with no air or foam layers and a substrate thickness of 3.175mm, it presents a 1-dB gain bandwidth of 33.52%. This is mainly due to the 5 parasitic dipoles unit cell used that can provide several resonances or degrees of freedom which contributes to a large reflection phase range of 800°. Moreover, there are two attempts to design wideband large RA in Ku-band listed in Table 2, such as those in [55] and [62] with aperture sizes of $42\lambda_0 * 39.6\lambda_0$ and $48\lambda_0 * 48\lambda_0$ at 12GHz, respectively. It is important to mention that the design presented in [62] is single layer while the one presented in [55] has three layers. Both designs use unit cells that provide reflection phase ranges larger than 360° to account for the spatial phase delay from the feed due to the large aperture size. The 1-dB gain bandwidth is similar with 10% and 12% in [55] and [62], respectively. On that account, considering the manufacturing complexity, it can be observed that the single layer RA in [62] would be preferred against a multilayer alternative with comparable performance. On the other hand, in terms of manufacturing tolerances, the simplicity of the square stacked patches presented in [55] would yield highest manufacturing accuracy as compared to the design presented in [62] which has more complex geometry of the concentric square and cross shaped loops. Consequently, the low gain bandwidth performance of the large RAs of [55] and [62], shows the difficulty in achieving wideband performance when the effect of the spatial phase delay from the feed to each element becomes more pronounced.

Another two RAs operating in Ku-band are the [63] and [65] with comparable aperture sizes of $8.7\lambda_0 * 8.7\lambda_0$ and $10\lambda_0 * 10\lambda_0$ at 13GHz and 13.5GHz,

respectively. However, the design in [63] presents a much lower bandwidth of 22.7% 3-dB gain bandwidth than the RA in [65] with a 1-dB gain bandwidth of 28.7%. Another important observation is that the design of [63] presents much lower AE (e.g., 50.2%) than the AE of [65] (e.g., 60.2%). The main reason of this large performance difference between the two RAs is that the design in [63] uses a substrate thickness of 1.5mm and an F/D of 2.35, while the one in [65] has double the thickness and a F/D of 1. As a result, the linearity of the reflection phase response in [65] is higher and hence the phase errors are minimized allowing for a larger gain-bandwidth.

The RA in [69] operates at two frequency namely Ku/K- band and achieves dual LP. The RA is illuminated by two feeds each corresponding to a different frequency. The antenna was able to generate the same radiation pattern for both orthogonal polarizations at each band with the capability of dual CP radiation if a dual CP feed is employed. The 2-dB gain bandwidth for the Ku-band and K-band is 20% and 5%, respectively The main limitations faced by the authors was the grating lobes that appeared in the Ka-band which is mainly attributed to edge cells having higher order propagating Floquet modes. Apart from that, the mutual coupling between parallel dipoles was another challenge in achieving independent phase and polarization control in each frequency band. The same unit-cell concept of printed dipoles was also followed in [71] to realize a broadband RA with high polarization purity for 4K and 8K UHDTV DVB-S2 applications. A broadband performance of 20% bandwidth and a crosspolar isolation of 37dB was achieved where the crosspolar isolation is consider as the ratio between the minimum copolar and maximum crosspolar gain withing the coverage area. The high purity in polarization was attributed to the optimization routine adapted. The routine was divided into stages with the orthogonal polarizations optimized independently at each sub-stage considering the degrees of freedom offered by the unit-cell. At the final substage of each stage, the crosspol requirements were taken into account by utilizing up to 6 degrees of freedom per unit-cell

Finally, amongst all designs listed in Table 2, the only RA that operates in Q-band can be found in [54]. This wideband RA operates in the highest frequency as compared to all designs reported in Table 2. It presents a good 1-dB gain bandwidth performance of 29.3% which can be explained by the used dual resonance unit cell and the 1mm air layer employed in the substrate structure. However, the aperture efficiency is only 47% and the F/D used is 1.3. Designing RAs that operates at higher frequency bands such as Q-band can result in apertures that are electrically large without sacrificing the limited real estate of satellite platforms. As a result, high gains such as 31.9dBi at 45GHz and very good gain bandwidth performance can be achieved in a small form factor [54].

C. ANGULAR ROTATION APPROACH EVALUATION

There are 7 wideband RAs listed in Table 2 that utilize the element rotation approach as a wideband phase tuning technique. The RAs operate in X, Ku and Ka-band frequency range. As previously mentioned in subsection *A*, the element rotation approach is used to design wideband CP RAs, hence, it is of great importance to examine the joint AR and gain bandwidth of these designs.

The X-band RAs can be found in [74], [76] and [80]. The designs have an F/D greater than 0.97 to ensure a -10dB edge tapering on the RA aperture and present an AE of 60%. They have similar aperture sizes of $7\lambda_0 * 7\lambda_0$, $6.45\lambda_0 * 6.45\lambda_0$ and $6.5\lambda_0 * 6.5\lambda_0$ at 11.6GHz, 11GHz and 9.9GHz as seen in Table 2, respectively. However, the three designs have different aperture and substrate thickness as well as substrate material. More specifically, in [74] the authors use a relatively thin substrate of 0.5 mm with $\varepsilon_r = 3.55$ and a thick air layer of 4mm, while in [76] a lossy 1.5mm substrate with $\varepsilon_r = 4.4$ and a 2.2 mm thick foam layer was employed. On the other hand, the design in [80] has a thickness of 3mm and $\varepsilon_r = 3.66$ while it does not use any foam or air layer which makes this RA more attractive for 5G/6G applications where size and weight limitations are important. Furthermore, the double split ring with the I-shaped dipole used in [76], achieves better cross polarization suppression of -25dB as compared to -15dB for the S-shaped unit cell or the ME dipole unit cells. As suggested by the authors of [76], it is important to use a feed with excellent polarization purity and at the same time consider the magnitude of the cross polarized reflection coefficient. The authors of [74] highlighted that element such as the split circular or rectangular rings have narrowband cross-polarization suppression and thus fail to achieve a wide AR bandwidth. For this reason, they combined two different elements, the I-shaped dipole, and the double split ring to achieve a much wider cross polarization suppression as indicated by the reflection coefficient magnitude of the cross polarized field component. The designs in [74], [76] and [80] achieved a joint AR and gain bandwidth higher than 30 % as shown in Table 2 with [76] having the highest 3dB AR bandwidth of 68.5%. It is important to note that even though the design in [80] is a gap free aperture, it shows comparable performance in terms of AR and gain bandwidth with both [74] and [76].

From the designs that operate in Ku-band in [77] and [78], the RA in [78] shows superior 1-dB gain bandwidth performance of 35.8% as compared to 33.6% in [77]. This can be explained due to the larger aperture size and thinner substrate used in [77]. However, when the joint 3-dB AR and 1-dB gain bandwidth is considered, the 1-dB gain bandwidth of the RA in [78] is limited by its 3-dB AR bandwidth of 25.8%. Therefor the RA in [77] with a 3-dB AR bandwidth of 75% allows for a higher 1-dB gain bandwidth of 33.6%. Finally, there is one design that operates in the Ka-band [79], [81]. The RA in [79] has an aperture size of $9\lambda_0 * 9\lambda_0$ and achieves a joint 3-dB AR

and gain bandwidth of 24%. The only consideration of the proposed array is the multilayer structure and complexity of the cross-slot based unit cell. On the other hand the design in [81], has reduced complexity with a reduced aperture profile of $0.16\lambda_0$. The prototype RA was able to generate one RHCP and one LHCP reflected beam at 30GHz when illuminated by either a RHCP or LHCP wave respectively. Finally, the RA presents an excellent joint 1.5dB AR and 1-dB gain bandwidth of 30% at a center frequency of 30GHz.

D. TRUE TIME AND PHASE DELAY LINES APPROACH EVALUATION

As set out in Table 2, there are 6 wideband RA designs that use this approach. Most of these designs operate in X-band and they are presented in [82], [85], [86], [87], [88] and [89]. The works in [85], [86] and [87], [88] have comparable aperture sizes, see Table 2. However, the designs of [87], [88] are the only RAs from Table 2 which have an octagonal shaped aperture. Moreover, the RAs in [87], [88] present the best gain-bandwidth performance of 31.5%. It can also be observed that the RAs in [85] and [86], have similar 3-dB gain bandwidth performance of 18% and 17.8%, respectively. Nonetheless, the design in [86] is using a 3.175mm thick foam layer. An important observation is that the design of [85] presents the lowest AE efficiency of 35% as compared to all the RAs in Table 2. This can be explained due to the center fed configuration which gives rise to feed blockage. Moreover, the design in [82] is based on a unit cell of 4-layer aperture coupled TTD line and is able to achieve 1000° reflection phase range. The $27\lambda_0$ circular aperture RA achieves a 1.5dB gain bandwidth of 26.7%. The excellent gain-bandwidth performance for this large RA is mainly attributed to the TTD approach. Using this approach, the spatial phase delay can be accounted for by unit cells that can achieve reflection phases of multiples of 360°.The design in [89] operates in X and Ku-bands. The RA combines the split ring and phoenix patch element to achieve a 1-dB gain bandwidth of 20.7% and 12.9% in X and Ku band, respectively. To achieve these gain bandwidths, the reflection phase response must be independently designed on different frequency bands. The trade-off would be that multiband RAs will present a narrower bandwidth on each individual frequency band as compared to single band wideband RAs.

E. SUBWAVELENGTH PERIODICITY APPROACH EVALUATION

The subwavelength periodicity approach is the second most popular approach after the multi resonance, with 16 wideband RAs listed in Table 2. However, it is important to note that the subwavelength periodicity is the most flexible approach as it can be easily integrated with other approaches such as the element rotation, the multi resonance or phase delay lines to yield superior gain bandwidth characteristics as it will be discussed in Section IV-F. In this approach the majority of the designs operate in X-band [73], [93], [96]–[99], [101], [102]. There are one K-band designs [104], three Ku-band wideband RAs [95], [108], [100], one dual band RA at X/K-band [70] and two Ka-band designs [92], [94] while there are two tightly coupled RAs that operate in C-band and X-band, e.g., [107] and [105]. Different lattice periodicity can be observed from Table 2 such as $\lambda/3$, $\lambda/4$, $\lambda/5$ and $\lambda/6$.

Amongst all X-band RAs presented in Table 2, the RAs found in [99] and [102] have the smallest RA with size of $6.9\lambda_0 * 6.9\lambda_0$ at 10GHz and present the highest 1-dB gain bandwidth performance of 30% and 31%, respectively. Despite their large gain bandwidth, both unit cell designs are based on a single layer with no air or foam layer. In the case of [99], the subwavelength periodicity of $\lambda/3$ is combined with the phase delay lines approach to keep a satisfactory reflection phase range of 350°.On the other hand, the design in [102] has a finer grid periodicity of $\lambda/3 * \lambda/6$,hence it presents slightly lower achievable phase swing of 330° as compared to [99]. All the X-band RAs present excellent cross polarization suppression of higher than 20dB with the design in [99] reaching 32dB. On that account, [102] arranged the elements with mirror symmetry across the center line of the RA which greatly reduces the cross-polarized currents in the far-field, yielding cross-pol levels of −30dB. Moreover, the RA in [98] presents the highest AE as compared to all the designs listed in Table 2 which corresponds to 97.4% with F/D of 1.09 and has the smallest periodicity of $\lambda/6$. The authors stressed the fact that the geometrical similarity between neighboring scatterers across the reflective surface must be considered during the RA design as highly non-similar adjacent unit cells will violate the assumption of infinite periodic boundary conditions [51], [98]. Finally, the TTD subwavelength design in [101] offers the best balance between bandwidth performance and small grid periodicity. It presents a −3dB gain bandwidth of 40% while keeping the unit cell size as low as $\lambda/5$. The unique feature of this RA design lies on the way the phase profile is calculated.More specifically, the aperture is divided into zones where each zone must provide the required phase delay. Each time delay zone is treated as a homogenous slab where the parameter of interest is the refrective index and not the unit-cell dimensions. This methods allows for a macroscopic view of the RA where non-resonant element can be used. Consequently true-time delay performance with a linear phase response can be obtained at very fine grid arrangements.

From the RAs in Table 2, the design in [73] and [104] can achieve dual CP when illuminated by dual LP feed. The dual LP feed is either placed at +45° or −45° slant in respect to the unit cell axis to generate either a RHCP or LHCP beam, respectively. The proposed dual polarized Jerusalem Cross based RA achieved a −3dB AR bandwidth of 50% and −1dB gain bandwidth of 12.5% at X-band. The dual CP RA based on stacked patches achieved a 1-dB gain bandwidth of 20% and a 3-dB AR bandwidth of 19%.

The main difference between the two approaches for dual CP operation is that the design in [73] employs a single substrate layer compared to two layers in the design in [104].

From the Ku-band RAs, the authors of [100] introduced an alternative definition of bandwidth which is based on the ability of the RA to maintain an AE of more than 40%. Accordingly, the prototype RA achieved an AE bandwidth of 29% with a maximum AE of 70% and F/D of 0.9, see Table 2. Besides, the two Ka-band designs in [92] and [94] present small reflection phase ranges of 277° and 260°, respectively. A gain-bandwidth of [92] and [94] could not be compared as the design in [94] has a 0.5-dB gain bandwidth of 9.06% and the design in [92] has an 1-dB gain bandwidth of 19.6%. While both designs combine the subwavelength periodicity with the multi resonance, the main difference between these two designs is that [92] employs a stacked patch configuration while the one presented in [94] is using a single patch. To this end, the authors of [92] proved that by increasing the number of layers from 1 to 2, the gain-bandwidth can be increased by 4%. Additionally, the authors of [94] stressed that by reducing the subwavelength periodicity, the upper frequency bandwidth limit is affected, resulting in 3% improvement when the periodicity is reduced from $\lambda/2$ to $\lambda/3$. Nevertheless, the subwavelength periodicity will result in a limited reflection phase range which in turn will lead to phase errors and gain bandwidth degradation. A dual band dual LP X/K-band RA was proposed in [70]. The prototype RA was able to produce an X-polarized wave in the X-band and a Y-polarized wave in the K-band with a 1-dB gain bandwidth of more than 19% in both frequency bands. However, two different LP feeds were required to achieve dual polarization.

The tightly coupled RAs of [107] and [105] are evaluated in terms of their −10dB impedance bandwidth rather than the gain-bandwidth. Both designs are based on tightly coupled printed vertically arranged dipoles. The tightly coupled RAs are center fed and hence they would suffer from feed blockage. The design in [105] presents the highest impedance bandwidth of 31.2% while the one in [107] has a bandwidth of 25%. However, in [107], the authors managed to improve the AE by 20% as compared to [105] by using a variant-coupling -capacitance method and adjusting the F/D to 1.

F. COMPARISON OF THE APPROACHES AND DESIGN GUIDELINES

A wide bandwidth and flat reflection phase response was observed when a thick low loss substrate was used. Although this has the side effect of reducing the reflection phase response range which can cause phase errors and degrade the radiation performance of the RA. To account for this, unit cells that combine multiple resonances or true time delays can be employed to provide a reflection phase range in the excess of 360° and compensate for the extra phase swing required. The unit cell achievable reflection phase range is directly related to the wideband phase tuning technique employed. This can be observed in Table 2 where the TTD and the multi resonance multilayer approaches provide the largest reflection ranges up to 1000° [82] and 800° [55], [60], respectively. On the other hand, the subwavelength periodicity provides the smallest reflection phase ranges of 277° and 260° as indicated by [92] and [94]. On that account, most of the subwavelength RAs are combined with either the multi-resonance or the TTD approaches to compensate for the truncated phase swing.

In terms of polarization, the element rotation approach is the best choice for CP RAs showing AR bandwidths that reach 75% in [77] as compared to 11% and 28% when only the subwavelength periodicity [93] and the multi resonance [57] are used, respectively. From a unit cell design complexity perspective, the angular rotation is the simplest method for designing CP RAs as the element geometry remains unchanged and only the rotation angle is adjusted. On the other hand, by using either the multi resonance approach or the TTD or phase delay lines the element geometry varies according to the required reflection phase. In addition, considering the feeding method, the angular rotation technique is limited on the use of CP feeds while the multi resonance approach or the TTD or phase delay lines can produce CP reflected waves by either using a LP or CP feed. In the case of an LP feed, the unit cell must be properly designed to provide the required reflection phase as well as accommodate LP-to-CP conversion as illustrated in Fig. 11.

Moreover, the effect of the incident angel is an important factor that can contribute to phase errors and hence degrade the gain-bandwidth performance of the RA. This effect become more pronounced at the edge elements where the incidence angle deviates from the design specification which is even worse in the case of large RAs. Therefore, the elements in the center area will be illuminated with smaller incident angles as compared to the edge elements. From the investigated literature, it was found that both the reflection phase of the co- and cross polarized field components must be examined for oblique incidence angles up to 40° and must be considered in the phase profile distribution of the aperture. Nevertheless, a feed antenna tailored to the specific RA aperture and application can be designed and optimized to minimize these errors.

For large sized RAs where the aperture size exceeds $25\lambda_0$, the most suitable approach would be either the true time or phase delay lines or the multi resonance where multiple resonances are combined to realize a large enough phase swing counteracting for the spatial phase delay. Furthermore, the approach of true time or phase delay lines generates less phase errors as compared to the multi-resonance while the multi-resonance approach keeps the levels of the cross polarized radiation to a minimum.

In terms of AE and F/D, the unit cell rotation and the multi resonance approaches show the best average performances. Though, the highest recorded AE can be observed when the subwavelength approach is used as well. Slightly higher

gains can be achieved by using the subwavelength periodicity where the elements are arranged closer to each other. This means that more elements can fit in the same effective area and hence the gain of the RA can be improved. Metrics such as cross polarization and SLLs are mainly dictated by the application the RA is intended for and must be considered during the unit cell design phase. However, regardless of the approach used, the majority of the wideband RAs presented follow the seven design guidelines as outlined below:

1) 1-dB gain bandwidth exceeding 15%.
2) 3-dB AR bandwidth higher than 25% for CP designs.
3) At least 360° phase swing.
4) Linear reflection phase response.
5) Parallel phase versus variation, where variation depends on the approach used, for different frequencies.
6) Cross polarization levels both in the reflection coefficient magnitude and the radiation pattern must be kept below −15dB.
7) Side lobe levels below −20dB.

The best balance between gain bandwidth performance and RA complexity is observed when a combination of approaches is used as in the case of the multi resonance slotted rectangular patch with concave arm arranged in $\lambda/3$ [61], the rotated quasi-I-shaped unit cell with a $\lambda/4$ periodicity presented in [77] or the complete and split ring with a $\lambda/3$ periodicity proposed in [78]. As shown in Table 2, these designs achieve 1-dB gain bandwidth and AE exceeding 32% and 50% while satisfying the design guidelines of SLLs, cross polarization levels and using a single substrate layer. To conclude, it is essential to realize a large gain bandwidth performance by avoiding any air/foam layers or multilayer configurations. This is because, single layer wideband RAs would have a lower profile, higher structural fidelity, reduced cost and manufacturing complexity which are factors that are of great importance for satellite antennas.

V. CONCLUSION AND FUTURE TRENDS

In this paper wideband reflectarrays are surveyed both from a unit cell and a full system perspective with emphasis on the gain bandwidth performance. Four wideband approaches were investigated including the multi resonance approach, unit cell angular rotation, true time or phase delay lines and subwavelength periodicity. More specifically, the effect of the unit cell's geometry on the reflection phase response was considered. In the reflectarray system analysis, the following performance metrics were considered; the operating frequency, the reflection phase range, the substrate structure and material, the aperture size, the aperture efficiency, the focal distance, the cross-polarization performance as well as the gain and side lobe levels. It was found that the multi-resonance and the TTD approach can provide reflection phase responses exceeding 360°. Therefore, TTD or multi-resonance approach can be adopted in cases where wideband large size reflectarrays are needed such as base station or satellite terminal antennas. This is because the phase errors due to non-constant phase delay paths across the aperture can be offset by the additional phase delay provided by these approaches. In addition, thicker or multilayer substrates will normally limit the achievable reflection phase response. However, using the TTD or multi-resonance approach, thicker substrates or foam layer can be added which could potentially increase the linearity of the phase curve around resonance. For circular polarized wideband RAs, the unit cell angular rotation approach performs the best by achieving high joint AR and gain bandwidths. For dual polarized wideband reflectarrays, the choice of a common dual polarized or two single polarized feeds is a major cost and complexity factor. Nevertheless, when only a single approach was used to achieve wideband performance there is a trade-off between performance, complexity, and cost. Particularly, wide bandwidth was achieved when multiple dielectric, air and foam layers or highly complex unit cell geometries were employed. Though, the aforementioned design features present an increased cost as well as a high level of geometric complexity that may result in fabrication inaccuracies and phase errors especially in mmWave frequencies. Therefore, the best trade-off between gain bandwidth performance, cost and complexity were observed when either the multi resonance, unit cell angular rotation or TTD were combined with the subwavelength periodicity approach in a single layer reflectarray aperture.

As future directions for 5G/6G systems equipped with reflectarrays as enabling technology, research must be focused on mmWave reflectarrays where fabrication tolerances are strict, and the phase errors will become more pronounced. Along similar lines, new wideband reflectarray need to consider using single layer structures and incorporate the subwavelength periodicity in the design considerations. The next step would be to investigate the gain bandwidth of architectures that are capable of dual polarization and/or multi-band unit cells. In that case a wide gain bandwidth must be maintained in multiple frequency bands and/or polarizations. Finally, reconfigurable architectures where the unit cell contains active elements such as PIN diodes, varactors, liquid crystals or RF MEMs would be an inseparable feature of future 5G/6G systems. This is because reconfigurable reflectarrays are capable of beam scanning and polarization flexibility while maintaining a wide gain bandwidth while scanning the beam or when switching between polarizations would be a challenging task. Therefore, the bandwidth study on reconfigurable architectures could be another future research direction.

REFERENCES

[1] T. S. Rappaport *et al.*, "Millimeter wave mobile communications for 5G cellular: It will work!" *IEEE Access*, vol. 1, pp. 335–349, 2013, doi: 10.1109/ACCESS.2013.2260813.

[2] X. Artiga, J. Nunez-Martinez, A. Perez-Neira, G. J. L. Vela, J. M. F. Garcia, and G. Ziaragkas, "Terrestrial-satellite integration in dynamic 5G backhaul networks," in *Proc. 8th Adv. Satellite Multimedia Syst. Conf. 14th Signal Process. Space Commun. Workshop (ASMS/SPSC)*, Sep. 2016, pp. 1–6, doi: 10.1109/ASMS-SPSC.2016.7601470.

[3] S. Chen and J. Zhao, "The requirements, challenges, and technologies for 5G of terrestrial mobile telecommunication," *IEEE Commun. Mag.*, vol. 52, no. 5, pp. 36–43, May 2014, doi: 10.1109/MCOM.2014.6815891.

[4] H. Tataria, M. Shafi, A. F. Molisch, M. Dohler, H. Sjöland, and F. Tufvesson, "6G wireless systems: Vision, requirements, challenges, insights, and opportunities," *Proc. IEEE*, vol. 109, no. 7, pp. 1166–1199, Jul. 2021, doi: 10.1109/JPROC.2021.3061701.

[5] Y. J. Guo, M. Ansari, R. W. Ziolkowski, and N. J. G. Fonseca, "Quasi-optical multi-beam antenna technologies for B5G and 6G mmWave and THz networks: A review," *IEEE Open J. Antennas Propag.*, vol. 2, pp. 807–830, 2021, doi: 10.1109/OJAP.2021.3093622.

[6] J. Zhang, X. Ge, Q. Li, M. Guizani, and Y. Zhang, "5G millimeter-wave antenna array: Design and challenges," *IEEE Wireless Commun.*, vol. 24, no. 2, pp. 106–112, Apr. 2017, doi: 10.1109/MWC.2016.1400374RP.

[7] W. Hong *et al.*, "Multibeam antenna technologies for 5G wireless communications," *IEEE Trans. Antennas Propag.*, vol. 65, no. 12, pp. 6231–6249, Dec. 2017, doi: 10.1109/TAP.2017.2712819.

[8] I. F. Akyildiz, J. M. Jornet, and S. Nie, "A new CubeSat design with reconfigurable multi-band radios for dynamic spectrum satellite communication networks," *Ad Hoc Netw.*, vol. 86, pp. 166–178, Apr. 2019, doi: 10.1016/j.adhoc.2018.12.004.

[9] O. Kodheli *et al.*, "Satellite communications in the new space era: A survey and future challenges," *IEEE Commun. Surveys Tuts.*, vol. 23, no. 1, pp. 70–109, 1st Quart., 2021, doi: 10.1109/COMST.2020.3028247.

[10] F. Boccardi, R. W. Heath, A. Lozano, T. L. Marzetta, and P. Popovski, "Five disruptive technology directions for 5G," *IEEE Commun. Mag.*, vol. 52, no. 2, pp. 74–80, Feb. 2014, doi: 10.1109/MCOM.2014.6736746.

[11] B. Clerckx and C. Oestges, *MIMO in LTE, LTE-Advanced and WiMAX*. Amsterdam, The Netherlands: Elsevier, 2013, pp. 597–635.

[12] S. V. Hum and J. Perruisseau-Carrier, "Reconfigurable reflectarrays and array lenses for dynamic antenna beam control: A review," *IEEE Trans. Antennas Propag.*, vol. 62, no. 1, pp. 183–198, Jan. 2014, doi: 10.1109/TAP.2013.2287296.

[13] B. Imaz-Lueje, Á. F. Vaquero, D. R. Prado, M. R. Pino, and M. Arrebola, "Shaped-pattern reflectarray antennas for mm-wave networks using a simple cell topology," *IEEE Access*, vol. 10, pp. 12580–12591, 2022, doi: 10.1109/ACCESS.2022.3144915.

[14] P. Nayeri, F. Yang, and A. Z. Elsherbeni, "Introduction to reflectarray antennas," in *Reflectarray Antennas: Theory, Designs, and Applications*. New York, NY, USA: Wiley, 2018, pp. 1–8.

[15] J. Huang, "Analysis of a microstrip reflectarray antenna for microspacecraft applications," Jet Propulsion Lab., California Inst. Technol., Pasadena, CA, USA, Rep. 42-120, Feb. 1995.

[16] M. H. Dahri, M. H. Jamaluddin, M. I. Abbasi, and M. R. Kamarudin, "A review of wideband reflectarray antennas for 5G communication systems," *IEEE Access*, vol. 5, pp. 17803–17815, 2017, doi: 10.1109/ACCESS.2017.2747844.

[17] M. H. Dahri, M. I. Abbasi, M. H. Jamaluddin, and M. R. Kamarudin, "A review of high gain and high efficiency reflectarrays for 5G communications," *IEEE Access*, vol. 6, pp. 5973–5985, 2018, doi: 10.1109/ACCESS.2017.2786862.

[18] J. A. Encinar, C. Tienda, M. Barba, E. Carrasco, and M. Arrebola, "Analysis, design and prototyping of reflectarray antennas for space applications," in *Proc. Loughborough Antennas Propag. Conf. (LAPC)*, Nov. 2013, pp. 1–5, doi: 10.1109/LAPC.2013.6711840.

[19] R. Florencio, J. A. Encinar, R. R. Boix, V. Losada, and G. Toso, "Reflectarray antennas for dual polarization and broadband telecom satellite applications," *IEEE Trans. Antennas Propag.*, vol. 63, no. 4, pp. 1234–1246, Apr. 2015, doi: 10.1109/TAP.2015.2391279.

[20] R. Deng, S. Xu, F. Yang, and M. Li, "An FSS-backed Ku/Ka quad-band reflectarray antenna for satellite communications," *IEEE Trans. Antennas Propag.*, vol. 66, no. 8, pp. 4353–4358, Aug. 2018, doi: 10.1109/TAP.2018.2835725.

[21] M. Karimipour and I. Aryanian, "Demonstration of broadband reflectarray using unit cells with spline-shaped geometry," *IEEE Trans. Antennas Propag.*, vol. 67, no. 6, pp. 3831–3838, Jun. 2019, doi: 10.1109/TAP.2019.2902747.

[22] E. Martinez-de-Rioja *et al.*, "Advanced multibeam antenna configurations based on reflectarrays: Providing multispot coverage with a smaller number of apertures for satellite communications in the K and Ka bands," *IEEE Antennas Propag. Mag.*, vol. 61, no. 5, pp. 77–86, Oct. 2019, doi: 10.1109/MAP.2019.2932311.

[23] B. Imaz-Lueje, D. R. Prado, M. Arrebola, and M. R. Pino, "Reflectarray antennas: A smart solution for new generation satellite mega-constellations in space communications," *Sci. Rep.*, vol. 10, no. 1, 2020, Art. no. 21554, doi: 10.1038/s41598–020-78501–0.

[24] R. E. Hodges, D. J. Hoppe, M. J. Radway, and N. E. Chahat, "Novel deployable reflectarray antennas for CubeSat communications," in *Proc. IEEE MTT-S Int. Microw. Symp.*, May 2015, pp. 1–4, doi: 10.1109/MWSYM.2015.7167153.

[25] N. Chahat *et al.*, "Advanced CubeSat antennas for deep space and earth science missions: A review," *IEEE Antennas Propag. Mag.*, vol. 61, no. 5, pp. 37–46, Oct. 2019, doi: 10.1109/MAP.2019.2932608.

[26] M. Veljovic and A. K. Skrivervik, "Ultralow-profile circularly polarized reflectarray antenna for CubeSat intersatellite links in <italic>K</italic>-band," *IEEE Trans. Antennas Propag.*, vol. 69, no. 8, pp. 4588–4597, Aug. 2021, doi: 10.1109/TAP.2021.3060076.

[27] O. Kiris, K. Topalli, and M. Unlu, "A reflectarray antenna using hexagonal lattice with enhanced beam steering capability," *IEEE Access*, vol. 7, pp. 45526–45532, 2019, doi: 10.1109/ACCESS.2019.2909313.

[28] M. I. Abbasi, M. H. Dahri, M. H. Jamaluddin, N. Seman, M. R. Kamarudin, and N. H. Sulaiman, "Millimeter wave beam steering reflectarray antenna based on mechanical rotation of array," *IEEE Access*, vol. 7, pp. 145685–145691, 2019, doi: 10.1109/ACCESS.2019.2945318.

[29] S. Costanzo, F. Venneri, A. Borgia, and G. D. Massa, "Dual-band dual-linear polarization reflectarray for mmWaves/5G applications," *IEEE Access*, vol. 8, pp. 78183–78192, 2020, doi: 10.1109/ACCESS.2020.2989581.

[30] S. W. Qu, L. Xiao, H. Yi, B.-J. Chen, C. H. Chan, and E. Y.-B. Pun, "Frequency-controlled 2-D focus-scanning terahertz reflectarrays," *IEEE Trans. Antennas Propag.*, vol. 67, no. 3, pp. 1573–1581, Mar. 2019, doi: 10.1109/TAP.2018.2888949.

[31] M. A. ElMossallamy, H. Zhang, L. Song, K. G. Seddik, Z. Han, and G. Y. Li, "Reconfigurable intelligent surfaces for wireless communications: Principles, challenges, and opportunities," *IEEE Trans. Cogn. Commun. Netw.*, vol. 6, no. 3, pp. 990–1002, Sep. 2020, doi: 10.1109/TCCN.2020.2992604.

[32] X. Meng, M. Nekovee, and D. Wu, "The design and analysis of electronically reconfigurable liquid crystal-based reflectarray metasurface for 6G beamforming, beamsteering, and beamsplitting," *IEEE Access*, vol. 9, pp. 155564–155575, 2021, doi: 10.1109/ACCESS.2021.3125837.

[33] L. Zhang *et al.*, "A single-layer 10–30 GHz reflectarray antenna for the Internet of Vehicles," *IEEE Trans. Veh. Technol.*, vol. 71, no. 2, pp. 1480–1490, Feb. 2022, doi: 10.1109/TVT.2021.3134836.

[34] Z.-W. Miao, Z.-C. Hao, Y. Wang, B.-B. Jin, J.-B. Wu, and W. Hong, "A 400-GHz high-gain quartz-based single layered Folded reflectarray antenna for terahertz applications," *IEEE Trans. THz Sci. Technol.*, vol. 9, no. 1, pp. 78–88, Jan. 2019, doi: 10.1109/TTHZ.2018.2883215.

[35] P. Nayeri, F. Yang, and A. Z. Elsherbeni, "Reflectarray engineering and emerging applications," in *Reflectarray Antennas: Theory, Designs, and Applications*. Hoboken, NJ, USA: Wiley, 2018, pp. 367–400.

[36] P. Nayeri, F. Yang, and A. Z. Elsherbeni, "Beam-scanning reflectarray antennas: A technical overview and state of the art," *IEEE Antennas Propag. Mag.*, vol. 57, no. 4, pp. 32–47, Aug. 2015, doi: 10.1109/MAP.2015.2453883.

[37] M. H. Dahri, M. H. Jamaluddin, M. Khalily, M. I. Abbasi, R. Selvaraju, and M. R. Kamarudin, "Polarization diversity and adaptive beamsteering for 5G reflectarrays: A review," *IEEE Access*, vol. 6, pp. 19451–19464, 2018, doi: 10.1109/ACCESS.2018.2821358.

[38] M. H. Dahri *et al.*, "Aspects of efficiency enhancement in reflectarrays with analytical investigation and accurate measurement," *Electronics*, vol. 9, no. 11, p. 1887, 2020, doi: 10.3390/electronics9111887.

[39] J. Huang and R. J. Pogorzelski, "A Ka-band microstrip reflectarray with elements having variable rotation angles," *IEEE Trans. Antennas Propag.*, vol. 46, no. 5, pp. 650–656, May 1998, doi: 10.1109/8.668907.

[40] D. Berry, R. Malech, and W. Kennedy, "The reflectarray antenna," *IEEE Trans. Antennas Propag.*, vol. 11, no. 6, pp. 645–651, Nov. 1963, doi: 10.1109/TAP.1963.1138112.

[41] C. S. Malagisi, "Electronically scanned microstrip antenna array," U.S. Patent 4 053 895, 1977.

[42] T. A. Metzler, *Design and Analysis of a Microstrip Reflectarray*. Amherst, MA, USA: Univ. Massachusetts Amherst, 1993.

[43] D. M. Pozar and T. A. Metzler, "Analysis of a reflectarray antenna using microstrip patches of variable size," *Electron. Lett.*, vol. 29, no. 8, pp. 657–658, 1993.

[44] J. A. Encinar, "Design of two-layer printed reflectarrays using patches of variable size," *IEEE Trans. Antennas Propag.*, vol. 49, no. 10, pp. 1403–1410, Oct. 2001, doi: 10.1109/8.954929.

[45] A. Bhattacharyya, "Slot-coupled patch reflect array element for enhanced gain-band width performance," U.S. Patent 6 388 620 B1, 2002.

[46] M. Bozzi, S. Germani, and L. Perregrini, "Performance comparison of different element shapes used in printed reflectarrays," *IEEE Antennas Wireless Propag. Lett.*, vol. 2, pp. 219–222, 2003.

[47] D. M. Pozar, "Bandwidth of reflectarrays," *Electron. Lett.*, vol. 39, no. 21, pp. 1490–1491, 2003, doi: 10.1049/el:20030990.

[48] D. M. Pozar, "Wideband reflectarrays using artificial impedance surfaces," *Electron. Lett.*, vol. 43, no. 3, pp. 148–149, 2007, doi: 10.1049/el:20073560.

[49] N. Payam, Y. Fan, and Z. E. Atef, "Bandwidth of reflectarray antennas," in *Reflectarray Antennas: Theory, Designs, and Applications*. Hoboken, NJ, USA: Wiley, 2018, pp. 113–145.

[50] P. Nayeri, F. Yang, and A. Z. Elsherbeni, "Broadband and multiband reflectarray antennas," in *Reflectarray Antennas: Theory, Designs, and Applications*. Hoboken, NJ, USA: Wiley, 2018, pp. 179–225.

[51] L. Moustafa, R. Gillard, F. Peris, R. Loison, H. Legay, and E. Girard, "The phoenix cell: A new reflectarray cell with large bandwidth and rebirth capabilities," *IEEE Antennas Wireless Propag. Lett.*, vol. 10, pp. 71–74, 2011, doi: 10.1109/LAWP.2011.2108633.

[52] G. Ahmad, T. W. C. Brown, C. I. Underwood, and T. H. Loh, "An investigation of millimeter wave reflectarrays for small satellite platforms," *Acta Astronautica*, vol. 151, pp. 475–486, Oct. 2018, doi: 10.1016/j.actaastro.2018.06.044.

[53] M. E. Bialkowski and K. H. Sayidmarie, "Investigations into phase characteristics of a single-layer reflectarray employing patch or ring elements of variable size," *IEEE Trans. Antennas Propag.*, vol. 56, no. 11, pp. 3366–3372, Nov. 2008, doi: 10.1109/TAP.2008.2005470.

[54] X. Xia, Q. Wu, H. Wang, C. Yu, and W. Hong, "Wideband millimeter-wave microstrip reflectarray using dual-resonance unit cells," *IEEE Antennas Wireless Propag. Lett.*, vol. 16, pp. 4–7, 2017, doi: 10.1109/LAWP.2016.2551264.

[55] J. A. Encinar and J. A. Zornoza, "Broadband design of three-layer printed reflectarrays," *IEEE Trans. Antennas Propag.*, vol. 51, no. 7, pp. 1662–1664, Jul. 2003, doi: 10.1109/TAP.2003.813611.

[56] J. A. Encinar, M. Arrebola, L. F. de la Fuente, and G. Toso, "A transmit-receive reflectarray antenna for direct broadcast satellite applications," *IEEE Trans. Antennas Propag.*, vol. 59, no. 9, pp. 3255–3264, Sep. 2011, doi: 10.1109/TAP.2011.2161449.

[57] L. Ren, Y.-C. Jiao, F. Li, J.-J. Zhao, and G. Zhao, "A dual-layer T-shaped element for broadband circularly polarized reflectarray with linearly polarized feed," *IEEE Antennas Wireless Propag. Lett.*, vol. 10, pp. 407–410, 2011, doi: 10.1109/LAWP.2011.2148090.

[58] P. D. Vita, A. Freni, G. L. Dassano, P. Pirinoli, and R. E. Zich, "Broadband element for high-gain single-layer printed reflectarray antenna," *Electron. Lett.*, vol. 43, no. 23, pp. 1247–1249, 2007, doi: 10.1049/el:20072417.

[59] L. Li *et al.*, "Novel broadband planar reflectarray with parasitic dipoles for wireless communication applications," *IEEE Antennas Wireless Propag. Lett.*, vol. 8, pp. 881–885, 2009, doi: 10.1109/LAWP.2009.2028298.

[60] J. H. Yoon, Y. J. Yoon, W.-S. Lee, and J.-H. So, "Broadband microstrip reflectarray with five parallel dipole elements," *IEEE Antennas Wireless Propag. Lett.*, vol. 14, pp. 1109–1112, 2015, doi: 10.1109/LAWP.2015.2394810.

[61] M. Min and L. Guo, "Design of a wideband single-layer reflectarray antenna using slotted rectangular patch with concave arms," *IEEE Access*, vol. 7, pp. 176197–176203, 2019, doi: 10.1109/ACCESS.2019.2957840.

[62] M. R. Chaharmir, J. Shaker, N. Gagnon, and D. Lee, "Design of broadband, single layer dual-band large reflectarray using multi open loop elements," *IEEE Trans. Antennas Propag.*, vol. 58, no. 9, pp. 2875–2883, Sep. 2010, doi: 10.1109/TAP.2010.2052568.

[63] Q.-Y. Chen, S.-W. Qu, X.-Q. Zhang, and M.-Y. Xia, "Low-profile wideband reflectarray by novel elements with linear phase response," *IEEE Antennas Wireless Propag. Lett.*, vol. 11, pp. 1545–1547, 2012, doi: 10.1109/LAWP.2012.2232899.

[64] Q.-Y. Chen, S.-W. Qu, J.-F. Li, Q. Chen, and M.-Y. Xia, "An X-band reflectarray with novel elements and enhanced bandwidth," *IEEE Antennas Wireless Propag. Lett.*, vol. 12, pp. 317–320, 2013, doi: 10.1109/LAWP.2013.2249652.

[65] F. Xue, H.-J. Wang, M. Yi, G. Liu, and X.-C. Dong, "Design of a broadband single-layer linearly polarized reflectarray using four-arm spiral elements," *IEEE Antennas Wireless Propag. Lett.*, vol. 16, pp. 696–699, 2017, doi: 10.1109/LAWP.2016.2600374.

[66] X. Li, X. Li, Y. Luo, G. Wei, and X. Yi, "A novel single layer wideband reflectarray design using two degrees of freedom elements," *IEEE Trans. Antennas Propag.*, vol. 69, no. 8, pp. 5095–5099, Aug. 2021, doi: 10.1109/TAP.2021.3060098.

[67] H.-N. Hu, F.-P. Lai, and Y.-S. Chen, "Dual-band dual-polarized scalable antenna subarray for compact millimeter-wave 5G base stations," *IEEE Access*, vol. 8, pp. 129180–129192, 2020, doi: 10.1109/ACCESS.2020.3009431.

[68] S. Martin-Anton and D. Segovia-Vargas, "Fully planar dual-polarized broadband antenna for 3G, 4G and sub 6-GHz 5G base stations," *IEEE Access*, vol. 8, pp. 91940–91947, 2020, doi: 10.1109/ACCESS.2020.2994382.

[69] E. Martinez-de-Rioja, J. A. Encinar, M. Barba, R. Florencio, R. R. Boix, and V. Losada, "Dual polarized reflectarray transmit antenna for operation in Ku- and Ka-bands with independent feeds," *IEEE Trans. Antennas Propag.*, vol. 65, no. 6, pp. 3241–3246, Jun. 2017, doi: 10.1109/TAP.2017.2689059.

[70] X. Li, X. Li, and L. Yang, "Single-layer dual-band wide band-ratio reflectarray with orthogonal linear polarization," *IEEE Access*, vol. 8, pp. 93586–93593, 2020, doi: 10.1109/ACCESS.2020.2986040.

[71] D. R. Prado, M. Arrebola, M. R. Pino, and G. Goussetis, "Broadband reflectarray with high polarization purity for 4K and 8K UHDTV DVB-S2," *IEEE Access*, vol. 8, pp. 100712–100720, 2020, doi: 10.1109/ACCESS.2020.2999112.

[72] S. S. Gao, Q. Luo, and F. Zhu, "Introduction to circularly polarized antennas," *Circularly Polarized Antennas*. Hoboken, NJ, USA: Wiley, Jan. 22, 2014, pp. 1–28, doi: 10.1002/9781118790526.ch1.

[73] G.-B. Wu, S.-W. Qu, S. Yang, and C. H. Chan, "Broadband, single-layer dual circularly polarized reflectarrays with linearly polarized feed," *IEEE Trans. Antennas Propag.*, vol. 64, no. 10, pp. 4235–4241, Oct. 2016, doi: 10.1109/TAP.2016.2593873.

[74] L. Zhang, S. Gao, Q. Luo, W. Li, Y. He, and Q. Li, "Single-layer wideband circularly polarized high-efficiency reflectarray for satellite communications," *IEEE Trans. Antennas Propag.*, vol. 65, no. 9, pp. 4529–4538, Sep. 2017, doi: 10.1109/TAP.2017.2722824.

[75] A. Yu, F. Yang, A. Z. Elsherbeni, J. Huang, and Y. Kim, "An offset-fed X-band reflectarray antenna using a modified element rotation technique," *IEEE Trans. Antennas Propag.*, vol. 60, no. 3, pp. 1619–1624, Mar. 2012, doi: 10.1109/TAP.2011.2180299.

[76] M.-Y. Zhao, G.-Q. Zhang, X. Lei, J.-M. Wu, and J.-Y. Shang, "Design of new single-layer multiple-resonance broadband circularly polarized reflectarrays," *IEEE Antennas Wireless Propag. Lett.*, vol. 12, pp. 356–359, 2013, doi: 10.1109/LAWP.2013.2250245.

[77] W.-L. Guo, G.-M. Wang, K.-Y. Liu, Y.-Q. Zhuang, and Q.-C. Ge, "Design of single-layered ultrawideband high-efficiency circularly polarized reflectarray," *IEEE Antennas Wireless Propag. Lett.*, vol. 17, no. 8, pp. 1386–1390, Aug. 2018, doi: 10.1109/LAWP.2018.2846663.

[78] Q. Gao, J. Wang, Y. Li, and Z. Li, "A multiresonant element for bandwidth enhancement of circularly polarized reflectarray antennas," *IEEE Antennas Wireless Propag. Lett.*, vol. 17, no. 5, pp. 727–730, May 2018, doi: 10.1109/LAWP.2018.2808943.

[79] A. Mahmoud, A. A. Kishk, Z. Hao, and W. Hong, "Ka-band circularly polarized reflectarray: Using a double-layers cross slot," *IEEE Antennas Propag. Mag.*, vol. 58, no. 4, pp. 60–68, Aug. 2016, doi: 10.1109/MAP.2016.2569428.

[80] F. Wu, J. Wang, Y. Zhang, W. Hong, and K.-M. Luk, "A broadband circularly polarized reflectarray with magneto-electric dipole elements," *IEEE Trans. Antennas Propag.*, vol. 69, no. 10, pp. 7005–7010, Oct. 2021, doi: 10.1109/TAP.2021.3070653.

[81] Z. H. Jiang, Y. Zhang, and W. Hong, "Anisotropic impedance surface-enabled low-profile broadband dual- circularly polarized multibeam reflectarrays for *Ka*-band applications," *IEEE Trans. Antennas Propag.*, vol. 68, no. 8, pp. 6441–6446, Aug. 2020, doi: 10.1109/TAP.2020.2975263.

[82] E. Carrasco, J. A. Encinar, and M. Barba, "Bandwidth improvement in large reflectarrays by using true-time delay," *IEEE Trans. Antennas Propag.*, vol. 56, no. 8, pp. 2496–2503, Aug. 2008, doi: 10.1109/TAP.2008.927559.

[83] S. Costanzo, F. Venneri, and G. D. Massa, "Bandwidth enhancement of aperture-coupled reflectarrays," *Electron. Lett.*, vol. 42, no. 23, pp. 1320–1321, 2006, doi: 10.1049/el:20062492.

[84] F. Venneri, S. Costanzo, G. Di Massa, and G. Amendola, "Aperture-coupled reflectarrays with enhanced bandwidth features," *J. Electromagn. Waves Appl.*, vol. 22, nos. 11–12, pp. 1527–1537, 2008, doi: 10.1163/156939308786390247.

[85] H. Hasani, M. Kamyab, and A. Mirkamali, "Broadband reflectarray antenna incorporating disk elements with attached phase-delay lines," *IEEE Antennas Wireless Propag. Lett.*, vol. 9, pp. 156–158, 2010, doi: 10.1109/LAWP.2010.2044473.

[86] Y. Li, M. E. Bialkowski, and A. M. Abbosh, "Single layer reflectarray with circular rings and open-circuited stubs for wideband operation," *IEEE Trans. Antennas Propag.*, vol. 60, no. 9, pp. 4183–4189, Sep. 2012, doi: 10.1109/TAP.2012.2207060.

[87] C. Han, Y. Zhang, and Q. Yang, "A novel single-layer unit structure for broadband reflectarray antenna," *IEEE Antennas Wireless Propag. Lett.*, vol. 16, pp. 681–684, 2017, doi: 10.1109/LAWP.2016.2598733.

[88] C. Han, Y. Zhang, and Q. Yang, "A broadband reflectarray antenna using triple gapped rings with attached phase-delay lines," *IEEE Trans. Antennas Propag.*, vol. 65, no. 5, pp. 2713–2717, May 2017, doi: 10.1109/TAP.2017.2679493.

[89] T. Su, X. Yi, and B. Wu, "X/Ku dual-band single-layer reflectarray antenna," *IEEE Antennas Wireless Propag. Lett.*, vol. 18, no. 2, pp. 338–342, Feb. 2019, doi: 10.1109/LAWP.2018.2890766.

[90] C. Dau-Chyrh and H. Ming-Chih, "Multiple-polarization microstrip reflectarray antenna with high efficiency and low cross-polarization," *IEEE Trans. Antennas Propag.*, vol. 43, no. 8, pp. 829–834, Aug. 1995, doi: 10.1109/8.402202.

[91] E. Almajali, D. A. McNamara, J. Shaker, and M. R. Chaharmir, "Observations on the performance of reflectarrays with reduced inter-element spacings," in *Proc. IEEE Int. Symp. Antennas Propag. (APSURSI)*, 2011, pp. 369–372, doi: 10.1109/APS.2011.5996720.

[92] P. Nayeri, F. Yang, and A. Z. Elsherbeni, "Broadband reflectarray antennas using double-layer subwavelength patch elements," *IEEE Antennas Wireless Propag. Lett.*, vol. 9, pp. 1139–1142, 2010, doi: 10.1109/LAWP.2010.2094178.

[93] G. Zhao, Y.-C. Jiao, F. Zhang, and F.-S. Zhang, "A subwavelength element for broadband circularly polarized reflectarrays," *IEEE Antennas Wireless Propag. Lett.*, vol. 9, pp. 330–333, 2010, doi: 10.1109/LAWP.2010.2047836.

[94] P. Nayeri, F. Yang, and A. Z. Elsherbeni, "A broadband microstrip reflectarray using sub-wavelength patch elements," in *Proc. IEEE Antennas Propag. Soc. Int. Symp.*, Jun. 2009, pp. 1–4, doi: 10.1109/APS.2009.5171593.

[95] J. Ethier, M. R. Chaharmir, and J. Shaker, "Novel approach for low-loss reflectarray designs," in *Proc. IEEE Int. Symp. Antennas Propag. (APSURSI)*, Jul. 2011, pp. 373–376, doi: 10.1109/APS.2011.5996721.

[96] P.-Y. Qin, Y. J. Guo, and A. R. Weily, "Broadband reflectarray antenna using subwavelength elements based on double square meander-line rings," *IEEE Trans. Antennas Propag.*, vol. 64, no. 1, pp. 378–383, Jan. 2016, doi: 10.1109/TAP.2015.2502978.

[97] B. Mohammadi *et al.*, "Enhanced reflectarray antenna using elements with reduced reflection phase sensitivity," *IEEE Antennas Wireless Propag. Lett.*, vol. 17, no. 7, pp. 1334–1338, Jul. 2018, doi: 10.1109/LAWP.2018.2845439.

[98] J. L. T. Ethier, D. A. McNamara, M. R. Chaharmir, and J. Shaker, "Reflectarray design with similarity-shaped fragmented sub-wavelength elements," *IEEE Trans. Antennas Propag.*, vol. 62, no. 9, pp. 4498–4509, Sep. 2014, doi: 10.1109/TAP.2014.2330578.

[99] H. Yu and L. Guo, "Broadband single-layer reflectarray antenna employing circular ring elements dented with sectorial slits," *IEEE Access*, vol. 7, pp. 165814–165819, 2019, doi: 10.1109/ACCESS.2019.2953103.

[100] R. Deng, S. Xu, F. Yang, and M. Li, "A single-layer high-efficiency wideband reflectarray using hybrid design approach," *IEEE Antennas Wireless Propag. Lett.*, vol. 16, pp. 884–887, 2017, doi: 10.1109/LAWP.2016.2613882.

[101] S. M. A. M. H. Abadi, K. Ghaemi, and N. Behdad, "Ultra-wideband, true-time-delay reflectarray antennas using ground-plane-backed, miniaturized-element frequency selective surfaces," *IEEE Trans. Antennas Propag.*, vol. 63, no. 2, pp. 534–542, Feb. 2015, doi: 10.1109/TAP.2014.2381231.

[102] P. Ning, M. Min, L. Guo, and W. Feng, "On the use of half-cut elements for single-layer wideband reflectarrays," *IEEE Antennas Wireless Propag. Lett.*, vol. 20, no. 6, pp. 943–947, Jun. 2021, doi: 10.1109/LAWP.2021.3067740.

[103] L. Guo, H. Yu, W. Che, and W. Yang, "A broadband reflectarray antenna using single-layer rectangular patches embedded with inverted L-shaped slots," *IEEE Trans. Antennas Propag.*, vol. 67, no. 5, pp. 3132–3139, May 2019, doi: 10.1109/TAP.2019.2900382.

[104] E. Martinez-de-Rioja, D. Martinez-de-Rioja, R. López-Sáez, I. Linares, and J. A. Encinar, "High-efficiency polarizer reflectarray antennas for data transmission links from a CubeSat," *Electronics*, vol. 10, no. 15, p. 1802, 2021. [Online]. Available: https://www.mdpi.com/2079–9292/10/15/1802

[105] W. Li, S. Gao, L. Zhang, Q. Luo, and Y. Cai, "An ultra-wide-band tightly coupled dipole reflectarray antenna," *IEEE Trans. Antennas Propag.*, vol. 66, no. 2, pp. 533–540, Feb. 2018, doi: 10.1109/TAP.2017.2772311.

[106] D. Cavallo, A. Neto, G. Gerini, A. Micco, and V. Galdi, "A 3- to 5-GHz wideband array of connected dipoles with low cross polarization and wide-scan capability," *IEEE Trans. Antennas Propag.*, vol. 61, no. 3, pp. 1148–1154, Mar. 2013, doi: 10.1109/TAP.2012.2231920.

[107] J. Wang, Y. Zhou, S. Gao, and Q. Luo, "An efficiency-improved tightly coupled dipole reflectarray antenna using variant-coupling-capacitance method," *IEEE Access*, vol. 8, pp. 37314–37320, 2020, doi: 10.1109/ACCESS.2020.2973574.

[108] J. Ethier, M. R. Chaharmir, and J. Shaker, "Loss reduction in reflectarray designs using sub-wavelength coupled-resonant elements," *IEEE Trans. Antennas Propag.*, vol. 60, no. 11, pp. 5456–5459, Nov. 2012, doi: 10.1109/TAP.2012.2207672.

[109] S. Mener, R. Gillard, R. Sauleau, A. Bellion, and P. Potier, "Dual circularly polarized reflectarray with independent control of polarizations," *IEEE Trans. Antennas Propag.*, vol. 63, no. 4, pp. 1877–1881, Apr. 2015, doi: 10.1109/TAP.2015.2398458.

[110] T. Smith, U. Gothelf, O. S. Kim, and O. Breinbjerg, "Design, manufacturing, and testing of a 20/30-ghz dual-band circularly polarized reflectarray antenna," *IEEE Antennas Wireless Propag. Lett.*, vol. 12, pp. 1480–1483, 2013, doi: 10.1109/LAWP.2013.2288995.

[111] L. Guo, P.-K. Tan, and T.-H. Chio, "Single-layered broadband dual-band reflectarray with linear orthogonal polarizations," *IEEE Trans. Antennas Propag.*, vol. 64, no. 9, pp. 4064–4068, Sep. 2016, doi: 10.1109/TAP.2016.2574920.

[112] H. Hasani, M. Kamyab, and A. Mirkamali, "Low cross-polarization reflectarray antenna," *IEEE Trans. Antennas Propag.*, vol. 59, no. 5, pp. 1752–1756, May 2011, doi: 10.1109/TAP.2011.2123071.

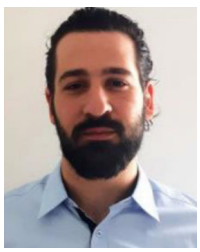

PANAGIOTIS (YANI) IOANNIS THEOHARIS (Graduate Student Member, IEEE) was born in Athens, Greece, in 1993. He received the B.Eng. degree (Hons.) in telecommunications engineering from the University of Wollongong, Wollongong, NSW, Australia, in 2018, where he is currently pursuing the Ph.D. degree under the Australian Government Research Training Program Scholarship. His research interests include antenna design for CubeSat applications, reconfigurable antennas, reflectarray antennas, and wearable antennas.

RAAD RAAD (Member, IEEE) received the Bachelor of Engineering degree (Hons.) in electrical engineering and the master's degree from the Switched Networks Research Centre, University of Wollongong, Wollongong, NSW, Australia, in 1997, and the Ph.D. degree in neuro-fuzzy logic admission control in cellular mobile networks, in 2006. Since 2004, he has been with the School of Electrical, Computer and Telecommunications Engineering, University of Wollongong, where he works as the Deputy Head of the School. His current research interests include wireless communications, CubeSat, the IoT, and antenna design. He received an Australian Postgraduate Award that was matched by Telstra Research Laboratories. He received a scholarship from the Motorola Australian Research Centre in the later part of his degree.

FAISEL TUBBAL (Senior Member, IEEE) received the B.E. degree from the College of Electronic Technology, Tripoli, Libya, in 2004, and the first M.S. degree in telecommunication engineering, the second M.S. degree in engineering management, and the Ph.D. degree in telecommunication engineering with the thesis titled "S-band Planar Antenna Designs for CubeSat Communications" from the University of Wollongong, Wollongong, NSW, Australia, in 2012, 2013, and 2017, respectively. He has been working as a Researcher with the Libyan Centre for Remote Sensing and Space Science, Tripoli. He joined the School of Electrical, Computer and Telecommunication Engineering, University of Wollongong, as an Academic Assistant in 2012. Since 2017, he has been a Casual Unit Conveyor with the School of Computing, Engineering and Mathematics, Western Sydney University, Australia. He was promoted to the position of Laboratory Manager with the School of Computer, Electrical and Telecommunication Engineering, University of Wollongong, in 2019. He is the Author of three chapters and more than 50 conference and journal papers. His research interests include antenna designs for CubeSat communications, wearable antennas, reconfigurable antennas, and antenna designs using metamaterials and metasurface antennas. He was a recipient of the Vice Chancellor's Awards for Outstanding Contribution to Teaching and Learning in 2016 and 2021. He is a Fellow of the Wollongong Academy for Tertiary Teaching and Learning Excellence.

MUHAMMAD USMAN ALI KHAN (Member, IEEE) received the B.Sc. and M.Sc. degrees in electronic engineering from the University College of Engineering and Technology, The Islamia University of Bahawalpur (IUB), Bahawalpur, Pakistan, in 2008 and 2013, respectively, and the Ph.D. degree from the School of Electrical, Computer and Telecommunication, University of Wollongong, Wollongong, NSW, Australia, where he is currently working on flexible wearable sensors and chipless RFID tags fabricated on polymer substrates, in collaboration with the Australian Institute for Innovative Materials. He is currently an Assistant Professor (study leave) with the Department of Electronic Engineering, IUB. His current research interests include flexible wearable devices for the Internet of Things, antenna design, and wireless communications.

ABBAS JAMALIPOUR (Fellow, IEEE) received the Ph.D. degree in electrical engineering from Nagoya University, Nagoya, Japan, in 1996. Since January 2022, he has been a Professor of Ubiquitous Mobile Networking with the University of Sydney. He has authored nine technical books, eleven book chapters, over 550 technical papers, and five patents, all in the area of wireless communications and networking. He was a recipient of the number of prestigious awards, such as the 2019 IEEE ComSoc Distinguished Technical Achievement Award in Green Communications, the 2016 IEEE ComSoc Distinguished Technical Achievement Award in Communications Switching and Routing, the 2010 IEEE ComSoc Harold Sobol Award, the 2006 IEEE ComSoc Best Tutorial Paper Award, as well as over 15 Best Paper Awards. He is the Editor-in-Chief of the IEEE TRANSACTIONS ON VEHICULAR TECHNOLOGY. He was the President of the IEEE Vehicular Technology Society from 2020 to 2021. Previously, he held the positions of the Executive Vice-President and the Editor-in-Chief of VTS Mobile World and has been an elected member of the Board of Governors of the IEEE Vehicular Technology Society since 2014. He was the Editor-in-Chief of IEEE WIRELESS COMMUNICATIONS, the Vice President-Conferences, and a member of Board of Governors of the IEEE Communications Society. He sits on the Editorial Board of the IEEE ACCESS and several other journals and is a member of Advisory Board of IEEE INTERNET OF THINGS JOURNAL. He has been the General Chair or The Technical Program Chair for several prestigious conferences, including IEEE ICC, GLOBECOM, WCNC, and PIMRC. He is a Fellow of the Institute of Electrical, Information, and Communication Engineers and the Institution of Engineers Australia, an ACM Professional Member, and an IEEE Distinguished Speaker.